Flow Turbulence Combust (2015) 94:381–414
DOI 10.1007/s10494-014-9585-x

RANS Simulations of Statistically Stationary Premixed Turbulent Combustion Using Flame Speed Closure Model

E. Yasari · S. Verma · A. N. Lipatnikov

Received: 2 June 2014 / Accepted: 9 November 2014 / Published online: 21 November 2014

Abstract Turbulent Flame Closure (TFC) and Flame Speed Closure (FSC) models of the influence of turbulence on premixed combustion are applied to RANS simulations of five sets of experiments with (i) highly turbulent, oblique, confined ONERA flames under elevated temperatures, (ii) highly turbulent, conical, confined PSI flames under elevated temperatures and pressures, (iii) open V-shaped flames, and weakly turbulent Bunsen (iv) Erlangen and (v) Orléans flames under the room conditions. Besides flame geometry, pressure, and initial temperature, bulk flow velocities, turbulence characteristics, and mixture compositions are different in these five sets of flames, with the equivalence ratio being varied in each set. Turbulence is modeled invoking either the standard or RNG $k - \varepsilon$ model. The same standard value $A = 0.5$ of a single constant of the TFC or FSC model is used in all these simulations, but certain input parameters of the turbulence model are tuned by investigating a single reference case for each set of flames. The TFC and FSC combustion models yield similar results when simulating the PSI flames, but the FSC model shows better performance in predicting burning rate for four other sets of flames. All in all, results computed using the FSC model agree reasonably well with the majority of the experimental data utilized to test the model, with a few exceptions discussed in the paper.

E. Yasari · A. N. Lipatnikov (✉)
Department of Applied Mechanics, Chalmers University of Technology, Gothenburg, 41296, Sweden
e-mail: lipatn@chalmers.se

E. Yasari
e-mail: yasari@chalmers.se

S. Verma
TimeTooth Technologies Pvt. Ltd., Noida, 201301, India
e-mail: salman.iaal@gmail.com

Keywords Premixed turbulent combustion · RANS simulation · Modeling · Validation · Flame Speed Closure

1 Introduction

Although a number of models for numerical simulations of the influence of turbulence on premixed burning have been proposed to be used, as reviewed elsewhere [1–5], the vast majority of them strongly need straightforward quantitative validation against experimental data obtained in a representative set of well-defined simple cases under substantially different conditions. From this perspective, the Turbulent Flame Closure (TFC) model [6–8], which is based on pioneering ideas by Prudnikov [9] and Zimont's theory of intermediately steady burning rate in turbulent flames with growing thickness [10], appears to be particularly promising, because the model has already been validated quantitatively by several independent research groups against experimental data obtained from various premixed turbulent flames, as reviewed elsewhere [1, 11].

By extending the TFC model in order to address weakly turbulent combustion and an early stage of premixed turbulent flame development, Lipatnikov and Chomiak [1, 12, 13] arrived at the so-called Flame Speed Closure (FSC) model. This extension of the TFC model was shown to be of importance when simulating expanding flames in bombs [1] or Spark Ignition (SI) piston engines [14]. However, contrary to the TFC model, application of the FSC model to statistically stationary turbulent burning associated e.g. with gas turbine engines has yet been very limited. The present authors are aware of a single paper [15] in that the FSC model was validated and compared with the TFC model in the case of statistically stationary premixed turbulent combustion, i.e. confined lean propane-air flames stabilized by a bluff body. Accordingly, the goal of the present work is to further study the FSC model and to compare it with the TFC model under statistically stationary conditions by numerically simulating five substantially different sets of premixed turbulent flames investigated experimentally by Moreau et al. [16–18], Dinkelacker and Hölzler [19], Siewert et al. [20, 21], Pfadler et al. [22], and Cohé et al. [23].

These five sets of experiments complement each other and were selected to test the models in a wide range of conditions, which cover (i) confined [16–18, 20, 21] and open [19, 22, 23] flames, (ii) various geometrical configurations (oblique [16–18], V-shaped [19], or conical [20–23] flames), (iii) room [19, 22, 23] and elevated [16–18, 20, 21] temperatures, (iv) room [16–19, 22, 23] and elevated [20, 21] pressures, (v) intense [16–18, 20, 21] and weak [19, 22, 23] turbulence, (vi) CH_4- [16–22] and CH_4/CO_2-air mixtures [23], (vii) measured transverse [17, 18] or axial [20, 23] profiles, flame heights [20, 22], or flame angles [19], (viii) various equivalence ratios, (ix) various Reynolds, Damköhler, and Karlovitz numbers, etc. Each of the studied sets of flames differs substantially from four others. The Bunsen flames investigated by Pfadler et al. [22] and Cohé et al. [23] are most close to one another, but different fuels were burned, different flame stabilization techniques were utilized, and different flame characteristics were reported.

In Section 2, the TFC and FSC models are summarized. Experiments used to test the two models and numerical setup are described in Section 3. Some general issues of validation of a combustion model using data obtained from statistically stationary premixed turbulent flames are discussed in Section 4. Results of testing the TFC and FSC models are addressed in Section 5, followed by conclusions.

2 TFC and FSC Models of Premixed Turbulent Combustion

2.1 The core of the models

Because both the TFC and FSC models were already discussed in detail in a couple of papers, e.g. see Refs. [1, 11, 24, 25], we will restrict ourselves to a brief summary of the two approaches. They (i) deal with the following well-known balance equation

$$\frac{\partial}{\partial t}\left(\bar{\rho}\tilde{c}\right) + \nabla \cdot \left(\bar{\rho}\tilde{\mathbf{u}}\tilde{c}\right) = -\nabla \cdot \overline{\rho \mathbf{u}'' c''} + \overline{W} \tag{1}$$

for the Favre-averaged combustion progress variable $\tilde{c}$ introduced by Bray and Moss [26], and (ii) provide the following joint closure relation

$$-\nabla \cdot \overline{\rho \mathbf{u}'' c''} + \overline{W} = \nabla \cdot [\bar{\rho}(\kappa + D_t)\nabla \tilde{c}] + \rho_u U_t \, |\nabla \tilde{c}| \tag{2}$$

for the two terms on the right hand side (RHS) of Eq. 1. Accordingly,

$$\frac{\partial}{\partial t}\left(\bar{\rho}\tilde{c}\right) + \nabla \cdot \left(\bar{\rho}\tilde{\mathbf{u}}\tilde{c}\right) = \nabla \cdot [\bar{\rho}(\kappa + D_t)\nabla \tilde{c}] + \rho_u U_t \, |\nabla \tilde{c}|. \tag{3}$$

Here, t is time, $\mathbf{u}$ is the flow velocity vector, ρ is the gas density, W is the mass rate of product creation, κ is the molecular heat diffusivity of the mixture, which is commonly neglected when using the TFC model, D_t and U_t are turbulent diffusivity and burning velocity, respectively, $\bar{q}$ is the Reynolds-averaged value of a quantity q with $q' \equiv q - \bar{q}$, whereas $\tilde{q} \equiv \overline{\rho q}/\bar{\rho}$ is the Favre-averaged value of a quantity q with $q'' \equiv q - \tilde{q}$.

Equation 3 was in fact introduced into the combustion literature by Prudnikov [9], but he wrote it in another form and applied it solely to statistically planar 1D flame that propagated in frozen turbulence. In the same 1D case, Eq. 3 was derived in Refs. [27, 28] by assuming that the mean structure of a developing premixed turbulent flame was self-similar, in line with various experimental data reviewed elsewhere [1, 9, 11]. Equation 3 yields permanent growth of the mean thickness δ_t of the aforementioned statistically planar 1D flame, whereas turbulent burning velocity does not depend on time to the leading order [9]. Such an intermediately asymptotic regime of premixed turbulent combustion pointed out by Prudnikov [9], Kuznetsov [29], Clavin and Williams [30], and Zimont [10] was later called "intermediate steady propagation (ISP) flames" [24].

In order to be consistent with this basic peculiarity of Eq. 3, a model for the turbulent burning velocity U_t, required to close the approach, should also address the ISP flames. To the best of the present authors' knowledge, the sole model that satisfies this basic requirement has yet been developed by Zimont [10], who has theoretically obtained the following expression

$$U_{t,ISP} = Au' Da^{1/4} = Au'^{3/4} S_L^{1/2} L^{1/4} \kappa_u^{-1/4}, \tag{4}$$

with $U_t = U_{t,ISP}$ being substituted into the second term on the RHS of Eq. 3 within the framework of the TFC model. Here, u' and L are the RMS turbulent velocity and an integral length scale of the turbulence, $Da = \tau_t/\tau_f$ is the Damköhler number, $\tau_t = L/u'$ and $\tau_f = \delta_L/S_L$ are the turbulence and flame time scales, respectively, S_L and $\delta_L = \kappa_u/S_L$ are the laminar flame speed and thickness, respectively, and A is a single model constant.

Equation 4 was derived under the following constraints [10, 24]; (i) the turbulent Reynolds number $\mathrm{Re}_t = u'L/\nu_u \gg 1$, (ii) the Damköhler number $Da \gg 1$, (iii) the Karlovitz number $Ka \propto (u'/S_L)^2 \mathrm{Re}_t^{-1/2} > 1$ and (iv) the flame-development time

$\tau_t < t_{fd} \ll \tau_t Da^{3/2}$. Subsequent tests of the TFC model, reviewed elsewhere [1, 11], have shown that it works well in a wider range of conditions, e.g. (ii′) $Da > 1$ and (iii′) $u' > S_L$.

2.2 Other elements of TFC model

To the best of the present authors' knowledge, in all RANS applications of the TFC model, (i) the turbulent diffusivity D_t in the first term on the RHS of Eq. 3 was associated with the fully developed turbulent diffusivity $D_{t,\infty}$ yielded by a turbulence model, e.g.

$$D_{t,\infty} = \frac{C_\mu}{Sc_t}\frac{\tilde{k}^2}{\tilde{\varepsilon}} \tag{5}$$

if the $k-\varepsilon$ model [31] is used, and (ii) the mean density was evaluated as follows

$$\bar{\rho} = \frac{\rho_u}{1+(\sigma-1)\tilde{c}}. \tag{6}$$

Here, k and ε are the turbulent kinetic energy and its dissipation rate, respectively, $C_\mu = 0.09$ is a constant of the $k-\varepsilon$ model [31], turbulent Schmidt number Sc_t will be discussed in Section 4.2, $\sigma = \rho_u/\rho_b$ is the density ratio and subscripts u and b designate unburned and burned gas, respectively. Note that Eq. 6 is valid not only in the well-known Bray-Mass-Libby (BML) case [26, 32] associated with a low probability γ of finding intermediate (between unburned and fully burned) states of the reacting mixture, but also in a general case provided that $c = (T-T_u)/(T_b-T_u)$ and, therefore, $1+(\sigma-1)c = \rho_u/\rho$. Indeed, Favre averaging of the latter equality results in Eq. 6.

When developing the TFC model [6–8], a quenching probability P_q

$$P_q = 1 - \frac{1}{2}\mathrm{erfc}\left\{-\frac{1}{\sqrt{2}\sigma_\varepsilon}\left[\ln\frac{\varepsilon_q}{\tilde{\varepsilon}} + \frac{\sigma_\varepsilon^2}{2}\right]\right\} \tag{7}$$

(or stretch-factor $G = 1 - P_q$) introduced by Bray [33] was incorporated into the RHS of Eq. 4 in order to address local combustion quenching by intense turbulent stretching, i.e. Eq. 4 was substituted with

$$U_{t,ISP} = Au'^{3/4}S_L^{1/2}L^{1/4}\kappa_u^{-1/4}(1-P_q). \tag{8}$$

Here, erfc is the complementary error function, $\sigma_\varepsilon^2 = 0.26\ln(L/\eta)$, $\eta = (\nu_u^3/\tilde{\varepsilon})^{1/4}$ is the Kolmogorov length scale, ν_u is the kinematic viscosity of unburned gas, $\varepsilon_q = 15\nu_u\dot{s}_q^2$, and $\dot{s}_q$ is a critical stretch rate associated with the local combustion quenching. Due to the lack of a model capable for predicting $\dot{s}_q$ and strong sensitivity of a stretched laminar premixed flame to the flame topology and transient effects, as reviewed elsewhere [34], the critical stretch rate is in fact an unknown input parameter of the quenching submodel given by Eq. 7. Therefore, the use of that submodel significantly reduces predictive capabilities of the TFC or FSC model. In all simulations discussed in the following, $P_q = 0$ (or $\varepsilon_q \to \infty$) unless a finite value of ε_q (or $\dot{s}_q$) is specified.

2.3 From TFC to FSC model

The FSC model is strongly based on the TFC model and involves the above equations, with P_q vanishing in all previous applications of the FSC model. In addition, the FSC model extends the TFC model in order to simulate an early stage of premixed turbulent flame development and weakly turbulent flames, as discussed in the rest of the present section.

2.3.1 Early stage of premixed turbulent flame development

Within the framework of the FSC model, growth of turbulent diffusivity and burning velocity during an early stage of premixed flame development is addressed following the classical theory of turbulent mixing by Taylor [35], which yields the following well-known expression

$$D_t = D_{t,\infty}\left[1 - \exp\left(-\theta_{fd}\right)\right] \equiv D_{t,\infty} f_1(\theta_{fd}) \tag{9}$$

for developing turbulent diffusivity in the simple case of a single point source of admixture. Subsequently, the following expression

$$U_t = U_{t,ISF}\left\{1 + \theta_{fd}^{-1}\left[\exp\left(-\theta_{fd}\right) - 1\right]\right\}^{1/2} \equiv U_{t,ISF} f_2(\theta_{fd}) \tag{10}$$

for developing turbulent burning velocity was derived [12] by combining the Taylor theory and the aforementioned model of $U_{t,ISF}$ by Zimont [10]. Here, $\theta_{fd} = t_{fd}u'^2/D_{t,\infty} \propto t_{fd}/\tau_t$ is the normalized flame-development time t_{fd}, while $U_{t,ISF}$ and $D_{t,\infty}$ are modeled by Eqs. 4 and 5, respectively.

The two extra terms $f_1(\theta_{fd})$ and $f_2(\theta_{fd})$, which pertain to the FSC model and describe the development of turbulent diffusivity and burning velocity, respectively, do not involve an empirical or tuning parameter. Both time-dependent terms tend to unity as $\theta_{fd} \to \infty$, i.e. the FSC Eqs. 9 and 10 reduce to the TFC Eqs. 5 and 4, respectively, in this limit case.

The flame-development time can easily be determined in the case of unsteady combustion initiated by a single spark. In this case, t_{fd} is simply counted from the ignition instant. When modeling a statistically stationary premixed turbulent flame, t_{fd} is still a meaningful quantity. Indeed, a statistically stationary flow can be a developing process, with the development occurring as a fluid particle is convected by the mean flow. Statistically stationary turbulence behind a grid develops, i.e. decays in the direction of the mean flow. A statistically stationary mixing layer develops, i.e. grows in the direction of the mean flow. Similarly, a statistically stationary premixed turbulent flame develops, i.e. both flame speed and mean flame brush thickness grow in the direction of the mean flow. In these cases, the turbulence (layer, or flame) development time is a field quantity, which is equal to the time required in order for a fluid particle to be convected from the grid (cross section associated with start of the mixing, or cross section where the flame is stabilized) to a point $\mathbf{x}$, i.e. $t_{fd} = t_{fd}(\mathbf{x})$.

In a general case, evaluation of t_{fd} is difficult. To resolve the problem, Zimont [36] has proposed to substitute Eq. 9 with a relaxation equation $dD_t/dt = u'^2(D_{t,\infty} - D_t)/D_{t,\infty}$ and to rewrite $U_t/U_{t,ISF}(\theta_{fd})$ given by Eq. 10 in a form of $U_t/U_{t,ISF}(D_t/D_{t,\infty})$ using Eq. 9. Such an approach has not yet been tested. In the present work, a simpler relation of $t_{fd} = x/U$ is invoked following Ref. [15]. Here, U is the mean flow velocity averaged over cross-section associated with flame stabilization and x is the distance from that cross-section, counted in the mean flow direction.

Note that an early stage of premixed turbulent flame development addressed by Eqs. 9 and 10 appears to play a substantial role in many statistically stationary laboratory flames. For instance, the TFC model yields $\delta_t \propto (D_{t,\infty}t_{fd})^{1/2} \propto (D_{t,\infty}x/U)^{1/2}$. The FSC model also predicts $\delta_t \propto (D_{t,\infty}x/U)^{1/2}$, but only if $\theta_{fd} \gg 1$, whereas $\delta_t \propto u't_{fd} \propto u'x/U$ at $\theta_{fd} \ll 1$. The latter (linear) dependence of δ_t on the distance x is well documented in various experiments reviewed elsewhere [11].

2.3.2 Weakly turbulent flames

In the simplest case of a statistically planar, 1D flow with frozen turbulence characteristics, the flame speed S_t yielded by the TFC model scales as $u'Da^{1/4}$ and vanishes as $u' \to 0$. Accordingly, the source term on the RHS of Eq. 3 also vanishes in this limit case, i.e. the TFC model cannot be applied to such a weakly turbulent flame.

To resolve the problem, the following laminar-like source term

$$Q_L = \frac{\bar{\rho}(1-\tilde{c})}{t_{ch}(1+D_t/\kappa_b)} \exp\left(-\frac{\Theta}{\tilde{T}}\right) \tag{11}$$

was incorporated [1, 12, 13] into the RHS of Eq. 3, which reads

$$\frac{\partial}{\partial t}(\bar{\rho}\tilde{c}) + \nabla \cdot \left(\bar{\rho}\tilde{\mathbf{u}}\tilde{c}\right) = \nabla \cdot [\bar{\rho}(\kappa + D_t)\nabla\tilde{c}] + \rho_u U_t |\nabla\tilde{c}| + Q_L \tag{12}$$

within the framework of the FSC model. Here, t_{ch} and Θ are the time scale and activation temperature, respectively, of a single reaction that combustion chemistry is reduced to, and the Favre-averaged temperature can easily be evaluated using the ideal gas state equation, i.e. $\bar{\rho}\tilde{T} = \rho_u T_u$. In intense turbulence associated with $\mathrm{Re}_t \to \infty$, a ratio of $D_t/\kappa_b \to \infty$ and, therefore, Q_L vanishes. In this limit case, the sole difference between the FSC and TFC models is associated with the two time-dependent terms on the RHSs of Eqs. 9 and 10.

If the laminar flame speed is known, then, the extra source term Q_L given by Eq. 11 does not involve a tuning parameter, because the time scale t_{ch} can easily be determined within the framework of the FSC model before running simulations of turbulent combustion. Indeed, if a typical value of Θ is set, e.g. 20 000 K in the present work, then, t_{ch} can be evaluated by (i) applying the FSC model to a planar 1D flame in the case of $u' = 0$ and (ii) finding t_{ch} such that the computed flame speed is equal to S_L, which is the key input parameter of both the TFC and FSC models. Because the computed flame speed scales as $(\kappa_u/t_{ch})^{1/2}$ if $u' = 0$, the pre-calculation of t_{ch} based on a known S_L requires only two iterations.

In the simplest case of a statistically planar, 1D flame that propagates in frozen turbulence, the FSC model yields turbulent flame speed S_t equal to $U_t + S_L$ [1, 12] and $S_t \to S_L$ as $u' \to 0$. Moreover, when $u' \to 0$, the turbulent diffusivity $D_t \to 0$ and the FSC Eq. 12 reduces to a well-known simple balance equation that models a laminar premixed flame in the case of a single global reaction. It is worth stressing, however, that the extra source term Q_L results solely from a linear interpolation between the latter balance equation valid at $u' = 0$ and the TFC balance equation valid at $Ka > 1$ or at least $u' > S_L$. Such a linear interpolation between two correct limit cases does not guarantee that the FSC model is a predictive approach at $0 < u' < S_L$. Accordingly, a particular goal of the present work consists of testing the FSC model under such weakly turbulent conditions.

A functional form of the dependence of turbulent burning velocity on u' and S_L in weakly turbulent flames is still an unresolved issue which was studied in many papers from the pioneering work by Damköhler [37] and Shchelkin [38] to very recent contributions [39, 40]. Although the simplest linear function was put into question by some experts [38, 40], recent DNS studies [41–43] supported it very well.

Because the extra term Q_L increases computed turbulent flame speed, the constant A, see Eq. 4, associated with the FSC model could be lower than the constant $A = 0.5$ determined using the TFC model [7, 8]. However, the term f_2 in Eq. 10 reduces the flame speed yielded by the former model. Because the opposite effects of Q_L and f_2 on S_t partially counterbalance one another, the difference in A_{FSC} and A_{TFC} does not seem to be large. In the present work, following Sathiah and Lipatnikov [15], we used $A_{FSC} = 0.5$ same as the

recommended value of A_{TFC} [7, 8]. Accordingly, subscripts FSC and TFC will be skipped when referring to the model constant A in the following.

3 Test Cases: Experiments and Numerical Setup

3.1 Range of flames and their characteristics

In the present work, numerical simulations of five sets of measurements are discussed. Experimental investigations of confined highly turbulent premixed flames, performed by Moreau et al. [16–18] and by Siewert et al. [20, 21], are selected, because (i) such flames are closely relevant to combustion in gas turbines and (ii) the extra source term Q_L given by Eq. 11 is expected to play a minor role in intense turbulence, thus, reducing the difference between the TFC and FSC models to the time-dependent terms $f_1(t)$ and $f_2(t)$ on the RHSs of Eqs. 9 and 10, respectively. The experiments by Moreau [17] were already simulated in order to test the TFC model [44–46], but a single lean flame was addressed in the cited numerical papers, whereas Moreau [17] investigated flames characterized by various equivalence ratios Φ. The present authors are not aware of RANS simulations of the measurements by Siewert et al. [20, 21], but these experiments were addressed using Large Eddy Simulation (LES) by Duwig et al. [47] and by Keppeler et al. [48], with both groups restricting themselves to a single equivalence ratio of $\Phi = 0.5$. Turbulent combustion models invoked in the two LES papers [47, 48] differed from one another and from the TFC or FSC model.

Open, weakly turbulent V-shaped [19] and Bunsen [22, 23] flames are selected, because (i) such flames are typical setup for applications of advanced laser diagnostic techniques to premixed turbulent combustion and (ii) differences between the TFC and FSC models should be more pronounced in weak turbulence due to a substantial role played by the extra source term Q_L. The experiments by Dinkelacker and Hölzler [19] were already simulated in order to test the TFC model [19, 46, 49], but the present authors are not aware of a simulation of more recent experiments by Pfadler et al. [22] or by Cohé et al. [23]. It is worth noting, however, that the methane-air flame investigated by Cohé et al. [23] was earlier studied by the same Orléans group [50] and the latter experiment was recently addressed in a LES work by Hernández-Pérez et al. [51].

Characteristics of all mixtures addressed in the present work are reported in Table 1, with the laminar flame speeds being computed by running PREMIX code [52] of CHEMKIN package [53] and invoking either GRI 3.0 [54] or Konnov's [55] chemical mechanism. The latter mechanism was used only when modeling experiments by Siewert et al. [20, 21].

Reported in Table 2 are ranges of variations in common non-dimensional characteristics of premixed turbulent flames, associated with each experimental investigation simulated in the present work. Here, the Karlovitz number $Ka = \mathrm{Re}_t^{1/2}/Da$. Due to lack of data on turbulence length scale in Ref. [17], the numbers Re_t, Da, and Ka were estimated using the length scale L set at the inlet boundary in our numerical simulations of the experiments by Moreau [17]. Due to significant spatial variations in the turbulence characteristics within the PSI burner [20], the estimates were performed using the values of u' and L measured in the non-reacting case in regions associated with the centerline positions of mean flame fronts in the counterpart reacting cases [20], as recommended by Daniele et al. [56]. For three other sets of flames, the values of u' and L were taken from Table 1 [19], Tables 2–3 [22], and Table 1 [23]. Table 2 indicates that flames simulated in the present work are associated with various regimes of premixed turbulent combustion.

Table 1 Mixture characteristicss

Fuel	Φ	P MPa	T_u K	T_b K	ρ_u/ρ_b	S_L m/s	κ_u cm^2/s	Flame configuration	Ref.
CH_4	0.62	0.1	600	1935	3.23	0.70	0.74	Oblique,	[17]
	0.80			2199	3.68	1.13		confined	
	0.83			2235	3.74	1.18			
	0.85			2258	3.78	1.21			
	0.87			2279	3.82	1.24			
	1.0			2274	4.01	1.35			
	1.24			2311	4.03	1.17			
CH_4	0.56	0.5	673	1890	2.81	0.325	0.179	Confined,	[20]
	0.50			1792	2.66	0.224		behind	
	0.47			1727	2.56	0.169		abrupt	
	0.43			1670	2.48	0.129		expansion	
	0.50	0.7		1792	2.66	0.189	0.128		
		1.0		1792	2.66	0.159	0.0897		
		1.5		1792	2.66	0.131	0.0598		
CH_4	0.50	0.1	298	1478	4.93	0.048	0.225	Open,	[19]
	0.58			1627	5.44	0.100		V-shaped	
	0.70			1839	6.18	0.195			
CH_4	0.57	0.1	298	1609	5.42	0.090	0.225	Open,	[22]
	0.60			1663	5.59	0.114		Bunsen	
	0.63			1716	5.76	0.138			
	0.65			1752	5.88	0.153			
	0.70			1839	6.18	0.195			
	0.75			1922	6.46	0.238			
	0.80			2000	6.72	0.278			
	0.85			2069	6.95	0.313			
	0.90			2137	7.20	0.347			
CH_4	0.60	0.1	298	1663	5.59	0.114	0.225	Bunsen	[23]
$0.1CO_2$+$0.9CH_4$				1651	5.50	0.105	0.223		
$0.2CO_2$+$0.8CH_4$				1637	5.45	0.098	0.222		
$0.35CO_2$+$0.65CH_4$				1608	5.36	0.084	0.219		

It is worth noting that the flames investigated by Pfadler et al. [22] are characterized by very low Reynolds numbers $\mathrm{Re}_t \leq 40$ and the Kolmogorov theory of turbulence is unlikely to be applicable to such flows. Because the derivation [10] of Eq. 4 was strongly based on the Kolmogorov theory, it would be too optimistic to expect that the TFC or FSC model, which invokes Eq. 4, can predict the basic characteristics of these flames. Nevertheless, simulations of the experiments by Pfadler et al. [22] were performed in order (i) to show limitations of the TFC or FSC model and (ii) to use well-documented data on scalar flux $\overline{\rho \mathbf{u}'' c''}$ reported in the cited paper in subsequent tests of a simple model of the flux, developed by Sabelnikov and Lipatnikov [57, 58]. Discussion of the latter model is, however, beyond the scope of the present paper.

Table 2 Non-dimensional flame characteristics

u'/S_L	Re_t	Da	Ka	Ref.
6–11.7	3800	20–71	0.9–3.2	[17]
9–30	1300–7000	2.3–15	2.6–22	[20]
1.3–5.4	90	2–36	0.30–4.4	[19]
0.4–1.6	15–40	6–89	0.05–0.8	[22]
1.3–1.8	85–131	30–34	0.27–0.31	[23]

3.2 Various cases

3.2.1 PSI experiments

In the experiment by Siewert et al. [20, 21], a lean preheated (673 K) methane-air turbulent flame was stabilized behind an abrupt expansion of a cylindrical channel, see Fig. 1. Measurements were performed for various elevated pressures ($P = 0.5 - 1.5$ MPa), air-fuel ratios $\lambda = 1.8 - 2.3$, i.e. the equivalence ratios $\Phi = 1/\lambda = 0.56 - 0.43$, and inlet bulk flow velocities $U = 30 - 60$ m/s. Moreover, inlet turbulence characteristics were varied by installing various grids in the incoming flow. The grids are shown in Fig. 1, where g350×g10 refers to a grid with a hole diameter $d_g = 3$ mm (the first digit 3) and a blockage ratio $b_g = 50$ % (the second and third digits 50), with the grid being mounted at $10 \times d_g$ (the last two digits 10) upstream in the inlet channel.

Turbulence characteristics were measured using Particle Image Velocimetry (PIV) techniques in constant-density non-reacting flows under atmospheric conditions. The spatial distributions of the Reynolds-averaged combustion progress variable were obtained by using OH Planar Laser Induced Fluorescence (PLIF) techniques and by statistically analyzing 800 single-shot 2D OH images. The mean centerline flame position X_{MP} was associated with the maximum of the probability density function $\mathcal{P}(x)$ of finding flame front at distance x, obtained by binarizing and averaging the aforementioned OH images. The mean flame brush thickness was evaluated as follows

$$\Delta X_{MP} = \frac{\max\{\mathcal{P}(x)\}}{\max\{d\mathcal{P}/dx\}}, \tag{13}$$

where $x \leq X_{MP}$.

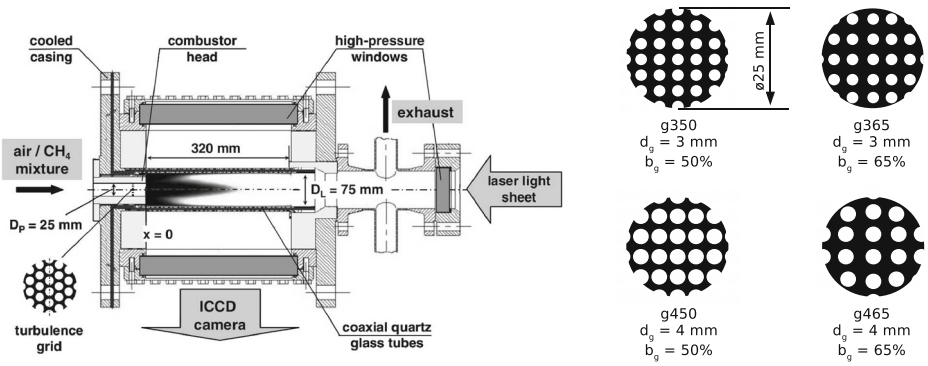

Fig. 1 PSI high-pressure combustion chamber and turbulence grids [20]

Reported in Ref. [20] are the values of X_{MP} and ΔX_{MP} obtained from various flames and three axial profiles of $\langle I_{OH} \rangle (x)$ obtained for three different equivalence ratios, with all other things being equal.

In order to simulate these experiments, the stationary, 2D, cylindrically symmetrical balance equations for the mass, momentum, turbulent kinetic energy, its dissipation rate, and the combustion model Eqs. 1–12 were numerically integrated using ANSYS FLUENT [59] until changes in all the variables in successive iterations were negligible. A pressure-based, segregated, solution procedure was employed, with pressure-velocity coupling being handled with SIMPLE algorithm. Pressure was interpolated using a second order method and the second-order upwind scheme was applied to the rest of the variables. Similarly to Duwig et al. [47], wall heat losses were not addressed, because Siewert [20] reported that (i) relative total heat losses decreased linearly from 10 % to 5 % when the pressure was increased from 0.5 to 1.5 MPa and (ii) the difference between the exit and adiabatic combustion temperatures was about 100 K at $P = 0.5$ MPa and was decreased with an increase in the pressure. Such moderate total wall heat losses are unlikely to significantly affect the axial profile of the Reynolds-averaged combustion progress variable, measured far from the walls.

In the simulations, the mean flame position X_{MP} was associated with a point on the centerline where the Reynolds-averaged combustion progress variable $\bar{c}$ was equal to 0.5. The mean thickness ΔX_{MP} of flame brush along the centerline was equal to the distance between the mean flame position and a point characterized by $\bar{c} = 0.05$. The Reynolds-averaged combustion progress variable was evaluated invoking the following BML equation [26]

$$\rho_b \bar{c} = \bar{\rho} \tilde{c}. \tag{14}$$

Grid sensitivity study was performed twice. First, in the cold flow reference case, the axial and radial profiles of velocity and u', computed using four different grids with uniform spacing of 0.9 (15 200 cells), 0.45 (60 000 cells), 0.22 (240 000 cells), and 0.11 (960 000 cells) mm, were compared with each other. The last two grids gave similar results and, similar profiles were obtained using a biased (towards the inlet and its edges) grid with an average cell size of 0.65 mm (28 000 cells).

Second, in the combustion reference case, the same axial profiles of the Reynolds-averaged combustion progress variable, see Fig. 4 in Section 4.3, were obtained using four biased grids consisting of 28 000, 37 310, 65 000, and 260 000 cells. Moreover, the same axial profile was computed in a single 3D case using a grid with 439 040 cells. Domain size sensitivity analysis was also performed by comparing the axial profiles of $\bar{c}$ calculated in two computation domains that had lengths of 320 and 640 mm. No differences between the two profiles were observed. Results reported in the following were computed using the biased grid with 28 000 cells in the former domain.

When simulating constant-density flows, six RANS turbulence models available in ANSYS FLUENT were tested, i.e. $k - \varepsilon$ model [31], RNG $k - \varepsilon$ model [60], realizable $k - \varepsilon$ model [61], $k - \omega$ model [62], shear-stress transport $k - \omega$ model [63], and FLUENT's Reynolds-stress model (http://aerojet.engr.ucdavis.edu/fluenthelp/html/ug/node1340.htm). Because the two versions of the $k - \omega$ model yielded worst agreement between computed and measured axial profiles of u', these two models were not applied to combustion simulations. While four other turbulence models, with all other things being equal, yielded different flame lengths, the differences were strongly reduced by setting different inlet dissipation rates for different models, see also Section 4.1. Results reported in the following were computed using the RNG $k - \varepsilon$ model [60] if the opposite is not stated. It is worth noting that the constant C_μ in Eq. 5 is equal to 0.0845 if the RNG $k - \varepsilon$ model is used.

The flow in the inlet channel was not simulated and the inlet boundary conditions were set at the channel nozzle using the following equations

$$\tilde{k} = \frac{3}{2}u'^2, \quad \tilde{\varepsilon} = C_D \frac{\tilde{k}^{3/2}}{L} = C'_D \frac{u'^3}{L} \tag{15}$$

and the values of the rms turbulent velocity and the longitudinal integral length scale L_{xx} for the axial velocity, reported by Siewert [20]. As discussed in Section 4.1, the constant C_D or C'_D is not known in a general case and requires tuning. Equation 15 was also used to evaluate u' and L in Eq. 4 based on the fields of $\tilde{k}(x,r)$ and $\tilde{\varepsilon}(x,r)$ computed within the combustion chamber. Here, r is the radial coordinate.

The radial profile of the mean axial velocity at the inlet was set as follows $\bar{u} = U(1-r/R)^q$, where R is the radius of the inlet channel, parameters U and q were evaluated using the measured bulk velocity and the mean axial velocity at the inlet center, reported by Siewert [20]. To check the sensitivity of computed results to the inlet boundary conditions for the mean velocity, simulations were also run by setting uniform $\bar{u}(r)$. Differences between X_{MP} obtained in simulations with non-uniform and uniform $\bar{u}(r)$ were small and were reduced by setting slightly different C_D in the two cases.

Wall function boundary conditions were set at all walls. Because the mean dissipation rate yielded by this method is typically high in the cell nearest to a wall, weak sensitivity of computed X_{MP} to variations in near-wall dissipation rate was checked using grids with different normalized near-wall distances y^+. At the outlet, fixed pressure boundary condition was set. Zero-gradient boundary condition was applied to the $\tilde{c}$-field at all boundaries with exception of the inlet, where $\tilde{c} = 0$.

3.2.2 *ONERA experiments*

Moreau [17] investigated oblique, confined, preheated (600 K), CH_4-air flames stabilized by a hot pilot flow of products in a planar combustion chamber, which had 100×100 mm square cross section and was 1300 mm long, see Fig. 2. The bottom flow of hot (2000 K) products and the flow of unburned mixture were separated by a splitter which was sufficiently thin (1 mm) in order to avoid the formation of a wake. The product flow inlet was 20 mm high and the cold flow inlet was 80 mm high. The mean flow velocities were equal to 120 and 60 m/s in the two inlets, respectively.

The rms axial velocity was measured [16] using Laser Doppler Anemometry (LDA). Radial profiles of the mean concentrations of CH_4, O_2, CO_2, and CO were measured using a sample probe.

Reported in Ref. [17] are a number of transverse profiles of the mean concentrations obtained from various flames at three distances x from the inlet and a few transverse profiles of the mean temperature, mean and rms axial velocity. In the present paper, we restrict

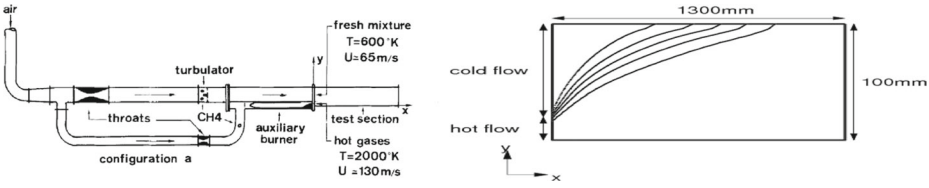

Fig. 2 Sketch of **a** ONERA combustion chamber [17] and **b** turbulent flame brush

ourselves to the transverse profiles of $\tilde{c}(y)$ that was calculated by normalizing the measured concentration of CH_4 using the methane mass fraction $X_{CH_4,u}$ in the unburned gas, i.e. $\tilde{c} = 1 - \tilde{X}_{CH_4}/X_{CH_4,u}$.

Unsteady 2D Favre-averaged balance equations for the mass, momentum, turbulent kinetic energy, its dissipation rate, and the combustion model Eqs. 1–12 were numerically integrated using Open Field Operation and Manipulation (OpenFOAM) library, version 1.7.x [64], until a stationary solution was reached. OpenFOAM is a license-free, open-source, general-purpose CFD library, which has been attracting a lot of attention both from the academia and the industry and provides a range of second order accurate (both in space and time) finite volume solvers for handling various problems. In the present simulations, convection terms were discretized using limited second order central difference method. Pressure field was computed using a combination of SIMPLE and PISO methods.

Heat losses were ignored, because experimental study by Magre et al. [18] did not indicate notable influence of wall heat losses on the mean flame brush, which was stabilized 20 mm above the bottom wall.

Numerical results reported in the following were obtained using a uniform 350×25 grid, with the grid independence of these results being confirmed by using finer meshes of 650×50 and 1300×120 points. In a single reference case, 3D simulations were performed in order to confirm that results of 2D and 3D RANS computations were very close to one another.

Four RANS turbulent models implemented into OpenFOAM, i.e. $k-\varepsilon$ model [31], RNG $k-\varepsilon$ model [60], realizable $k-\varepsilon$ model [61], and Launder-Sharma model [65], were used. The highest (lowest) burning rates were obtained using the Launder-Sharma and realizable $k-\varepsilon$ models, respectively, with results yielded by the $k-\varepsilon$ and RNG $k-\varepsilon$ models being sufficiently close to one another. Differences in transverse profiles of the Favre-averaged combustion progress variable, computed invoking various turbulence models, with all other things being equal, were substantially reduced by setting different inlet dissipation rates for the invoked turbulence models. Because a study of turbulence within premixed flames is beyond the scope of the present paper, we will restrict ourselves to reporting results obtained using the $k-\varepsilon$ model [31].

The inflow values of $\tilde{k}$ were evaluated by Zimont et al. [44, 45] using data reported by Moreau et al. [16, 17]. The inflow values of $\tilde{\varepsilon}$ will be discussed in Section 4.1. Spatially uniform mean axial velocities (different for reactant and product flows) were set at the inlet in line with the experimental data reported by Moreau and Boutier [16], see solid curve in Fig. 4 in the cited paper. The inlet values of $\tilde{c}$ were equal to unity and zero in the product and reactant flows, respectively. Wall function boundary conditions were set at the walls. At the outlet, fixed pressure boundary condition and $\partial\tilde{c}/\partial x = 0$ were set.

The rms velocity u' and and length scale L in Eq. 4 were evaluated using Eq. 15.

3.2.3 Erlangen V-shaped flames

Dinkelacker and Hölzler [19] studied open, lean methane-air, V-shaped flames stabilized by a 2-mm wire placed 10 mm above the exit of a vertically mounted circular nozzle with a diameter of 40 mm. Turbulence was produced by a perforated plate placed 70 mm below the nozzle exit. The inflow mean turbulent kinetic energy and integral length scale were evaluated using LDA 5 mm above the burner exit. In the case considered here, they were equal to 0.1 m^2/s^2 and 5.4 mm, respectively.

The mean field $\bar{c}(x, y)$ was measured by averaging sets of 2D instantaneous density fields obtained using planar laser-induced Rayleigh scattering technique. By analyzing a

mean field $\bar{c}(x, y)$, a flame half angle φ was calculated to be equal to the angle between the flame axis and "the tangent line of the $\bar{c} = 0.5$ isocontour at a distance of 15, 30, or 45 mm from the flame holder" [19].

Reported in Ref. [19] are images of the mean fields $\bar{c}(x, y)$ and the dependencies of φ on Φ obtained for the mean inlet flow velocities of 1.85 and 3 m/s. Only the latter case will be discussed in the following, because the turbulent Reynolds number Re_t was very low in the former case.

Although a cylindrical nozzle was used in these experiments, Dinkelacker and Hölzler [19] pointed out that the flame geometry was almost planar due to flame stabilization with a wire. These authors claimed that results of their planar 2D and 3D computations were very close to one another [19].

Accordingly, in the present work, unsteady planar 2D Favre-averaged balance equations for the mass, momentum, turbulent kinetic energy, its dissipation rate, and the combustion model Eqs. 1–12, supplemented with the $k - \varepsilon$ turbulence model [31] and Eqs. 14–15, were numerically integrated using OpenFOAM until a stationary solution was reached. Convection terms were discretized using limited second order central difference method. Pressure field was computed using a combination of SIMPLE and PISO methods.

Due to the statistical symmetry of the problem, only a half of the flame was considered and symmetry boundary conditions were set at the centerline. The rectangular computational domain of 30×105 mm^2 was discretized using a grid of 15 760 cells. Independence of the results on the grid refinement and on the size of the computational domain was independently checked by using a finer grid of 30 980 cells and expanding the computational domain to 90×140 mm^2, respectively. In the case of the larger domain, the numerical grid consisted of 45 760 cells.

The inlet boundary conditions for $\tilde{c}$, $\tilde{u}$, $\tilde{k}$, and $\tilde{\varepsilon}$ were uniform following Dinkelacker and Hölzler [19] who not only performed the measurements, but also simulated them. In the vicinity of the wire, the boundary condition of $\tilde{c} = 1$ was set in order to stabilize the flame in the simulations while zero gradient boundary condition was applied to $\tilde{k}$ and $\tilde{\varepsilon}$. At side and outlet boundaries, outflow boundary condition with a fixed pressure value was applied. Wall function boundary condition was set at the nozzle wall.

3.2.4 Erlangen Bunsen flames

In the experiments by Pfadler et al. [22], conical lean methane-air flames characterized by various equivalence ratios were stabilized by a cylindrical rim near the nozzle of a typical Bunsen burner with diameter of 48 mm. Turbulence was generated by a perforated plate placed 100 mm upstream the nozzle. In order to obtain a flat-top flow profile at the nozzle, a tapered insert was placed downstream the plate.

Instantaneous two-dimensional velocity field and boundary between unburned and burned mixtures were recorded utilizing Conditioned Particle Image Velocimetry (CPIV), i.e. the velocity was measured by applying PIV techniques, whereas the boundary was associated with a drop of the density of seeding particles (TiO_2). Subsequently, the instantaneous value of the combustion progress variable was set equal to zero or unity in the unburned or burned gas, respectively. The first and second moments of the $\mathbf{u}(\mathbf{x})$ and $c(\mathbf{x})$ fields were obtained by averaging 256 instantaneous images in each particular case.

Two sets of measurements were performed either varying the equivalence ratio and keeping the same flow rate or varying the mass flow rate and keeping $\Phi = 0.7$. In the former set, the bulk axial velocity U was equal 1.7 m/s, the rms axial u' and radial v' velocities were equal to 0.18 and 0.13 m/s, respectively, the longitudinal integral length scale L for the axial

velocity was equal to 2.5 mm. These turbulence characteristics were measured at the flow axis 3 mm downstream the nozzle. In the latter set, $U = 1.4-2.2$ m/s, $u' = 0.10-0.23$ m/s, $v' = 0.10 - 0.18$ m/s, and $L = 2.4 - 3.2$ mm.

Reported in Ref. [22] is a large amount of data relevant to the behavior of the turbulent scalar flux $\overline{\rho \mathbf{u}'' c''}$. Because evaluation of the flux is beyond the scope of the TFC or FSC model, only measured flame heights are used for validation purposes in the present work. These heights were counted along the burner axis and were equal to distances from the nozzle to points characterized by $\tilde{c} = 0.1$, 0.5, or 0.9.

In order to simulate these experiments, unsteady, 2D, cylindrically symmetrical Favre-averaged balance equations for the mass, momentum, turbulent kinetic energy, its dissipation rate, and the combustion model Eqs. 1–12, supplemented with the $k - \varepsilon$ turbulence model [31] and Eq. 15, were numerically integrated using OpenFOAM until a stationary solution was reached. Convection terms were discretized using limited second order central difference method. Pressure field was computed using a combination of SIMPLE and PISO methods.

Results discussed in the following for tall flames ($\Phi \leq 0.75$) were computed using a mesh of 51 000 cells in an axisymmetric computational domain of a length of 200 mm and a radius of 24 mm. Independence of the results on the grid refinement was checked using grids of 37 400 and 70 000 cells. Shorter flames ($\Phi = 0.8$, 0.85, and 0.9) were simulated using a mesh of 98 800 cells in an axisymmetric computational domain of a length of 100 mm and a radius of 24 mm. Independence of the results on the grid refinement or the size of the computational domain was independently checked by using grids of 84 000 and 124 000 cells or by reducing the length of the computational domain to 70 mm.

The inlet boundary conditions for $\tilde{c}$, $\tilde{u}$, $\tilde{k}$, and $\tilde{\varepsilon}$ were uniform. The radial profile of the mean axial velocity measured 3 mm above the nozzle, see Fig. 2a in Ref. [22], is consistent with the uniform inlet condition. Axisymmetric boundary condition was set at the burner axis and outflow boundary condition with fixed pressure was applied at the outlet and side boundaries, where the gradient of $\tilde{c}$ was zero. In the vicinity of the rim, the boundary condition of $\tilde{c} = 1$ was set in order to stabilize the flame in the simulations.

3.2.5 Orléans experiments

Cohé et al. [23] stabilized axisymmetric turbulent CH_4/CO_2/air Bunsen flames at a nozzle of diameter of 25 mm within a cylindrical high pressure combustion chamber using an annular laminar stoichiometric methane-air pilot flame. The laminar pilot flame flow rate was much less (about 7 %) than the main turbulent flow rate. The bulk flow velocity of unburned mixture was equal to 2.1 m/s at various pressures.

Turbulence was generated by a perforated plate placed 50 mm upstream of the nozzle. Instantaneous velocities conditioned on the unburned mixture were measured by seeding the incoming flow with olive oil droplets and applying Laser Doppler Velocimetry (LDV) techniques. According to Table 1 in [23], the rms axial and radial components of the flow velocity vector were equal to 0.15 and 0.12 m/s, respectively. The reported integral length scale was increased from 9 to 13.9 mm when the volume percent of CO_2 was increased from 0 to 35 at $P = 0.1$ MPa.

Instantaneous 2D images of the unburned gas were collected by recording laser induced Mie scattering. Cohé et al. [23] reported centerline axial profiles of the Reynolds-averaged combustion progress variable $\bar{c}(x)$, which were obtained by binarizing 300 images in each particular case, followed by averaging the binarized images.

In order to simulate these experiments, unsteady, 2D, cylindrically symmetrical Favre-averaged balance equations for the mass, momentum, turbulent kinetic energy, its dissipation rate, and the combustion model Eqs. 1–12, supplemented with the $k - \varepsilon$ turbulence model [31] and Eqs. 14–15, were numerically integrated using OpenFOAM until a stationary solution was reached. Convection terms were discretized using limited second order central difference method. Pressure field was computed using a combination of SIMPLE and PISO methods.

Results discussed in the following were computed using a mesh of 70 000 cells in an axisymmetric computational domain with a length of 200 mm and a radius of 15 mm. Independence of the results on the grid refinement or the size of the computational domain was independently checked by using grids of 51 000 and 100 000 cells or by decreasing the length of the computational domain to 150 mm, respectively.

The inlet boundary conditions for $\tilde{u}$, $\tilde{k}$, and $\tilde{\varepsilon}$ were uniform, whereas $\tilde{c} = 0$ and 1 in reactant flow and product co-flow, respectively. Axisymmetric boundary condition was set at the burner axis and outflow boundary condition with fixed pressure was applied at the outlet and side boundaries, where $\tilde{c} = 1$.

4 Validation and Tuning

The FSC (or TFC) combustion model involves a single[1] constant A, see Eq. 4, that was neither tuned nor varied in the present work. Nevertheless, testing the model was not free from tuning. The point is that, in order to assess any combustion model in RANS simulations of statistically stationary premixed turbulent flames, one has to evaluate u', L, and turbulent diffusivity $D_{t,\infty}$. To do so, proper models of turbulence and turbulent mixing should be invoked. Accordingly, computed flame characteristics are affected not only by the combustion model, but also by turbulence and mixing models, their constants, and boundary conditions relevant to the latter models.

As reviewed elsewhere [66], predictive models of various effects associated with the influence of premixed combustion on turbulence have not yet been developed. Moreover, even consistent characterization of turbulence within premixed flame brush is an issue [67, 68]. Accordingly, a common practice consists of invoking models of turbulence and mixing[2] that are widely used in simulations of constant-density non-reacting flows, e.g. the $k - \varepsilon$ model of turbulence [31] and Eq. 5. However, even such a strongly simplified method involves input parameters that are case-dependent and require tuning, as discussed in the rest of the present section.

4.1 Dissipation rate

To simulate a turbulent flow, the value of the dissipation rate at the inflow boundary is required, at least if the $k - \varepsilon$ model is invoked. Such a value is not specified in a typical paper that reports experimental data obtained from a premixed flame. On the face of it, the inlet value of $\tilde{\varepsilon}$ could be evaluated by substituting the measured value of L into Eq. 15. However, such a solution is neither simple nor straightforward.

[1] $P_q = 0$ in all simulations with a single exception discussed later.

[2] The use of the gradient diffusion term on the RHS of Eq. 2 does not mean that the flux $\overline{\rho \mathbf{u}'' c''}$ is closed by invoking the gradient diffusion approximation. Equation 2 is a joint closure of two terms and is consistent with eventual countergradient behavior of the flux $\overline{\rho \mathbf{u}'' c''}$, as shown elsewhere [58, 69].

First, in some experimental papers, e.g. [17], there are no data on an integral length scale L. To simulate such experiments, the length scale can be either set with an order-of-magnitude precision or tuned.

Second, even if a length scale L is specified, the reported information is often incomplete, e.g. [19, 23]. The point is that a single integral length scale L is insufficient to characterize a turbulent flow. In a general case, there are nine different Eulerian integral length scales L_{ij} measured for the i-th component of the flow velocity vector in the j-th direction [70]. Moreover, turbulent mixing is characterized by Lagrangian length scales $L_{L,i}$, which differ from the Eulerian L_{ij}.

Third, even if complete information is provided, e.g. reported in [20, 22] are the Eulerian scales L_{11}, the "constant" C_D is poorly known and is not constant [70]. In commercial CFD codes, the default value of C_D is commonly equal to $C_\mu^{3/4}$, i.e. 0.165 if the $k-\varepsilon$ model is used. However, such a choice of C_D is poorly justified. In the simplest case of isotropic turbulence, an increase in C_D with decreasing Reynolds number is well documented in DNS [71–74], with the effect being strongly pronounced at low Re_t. These DNS data imply that C_D tends to a finite constant value $C_{D,\infty}$ as $\mathrm{Re}_t \to \infty$, but this asymptotic value depends on "details of forcing at low wavenumbers" [72] and $C_{D,\infty}$ reported in the cited DNS papers varies from 0.22 [74] to 0.37 [72], whereas Pope [70] set $C_{D,\infty} = 0.43$, see p. 244 in his book. In an anisotropic turbulent flow associated with a typical burner, evaluation of C_D is even more difficult.

When simulating a particular combustion experiment, either C_D or a ratio of C_D/L in Eq. 15 could be evaluated by comparing results computed for various inlet $\tilde{\varepsilon}$ with experimental data obtained from the non-reacting cold flow. Such a solution is satisfactory provided that (i) used RANS turbulence model well predicts the measured data and (ii) computed results are sufficiently sensitive to the inlet $\tilde{\varepsilon}$. This is not the case for many flows. For instance, the axial profiles of the mean $\bar{u}(x)$ and rms $u'(x)$ axial velocities, measured by Siewert [20] in a cold flow in the PSI burner, agree equally "well" with results computed for various inlet $\tilde{\varepsilon}$, see Fig. 3. The constant C_D associated with the best agreement between measured and computed $\bar{u}(x)$ differs from C_D associated with the best agreement between measured and computed $u'(x)$.

Moreover, cold flow data are not always provided, e.g. [22, 23].

Furthermore, even if the inlet value of $\tilde{\varepsilon}$ is well determined by experimentally (and numerically) investigating a cold flow, it is still insufficient to simulate premixed combustion. The knowledge of the inlet $\tilde{\varepsilon}$ allows one to compute the fields of $u'(\mathbf{x})$, $\tilde{k}(\mathbf{x})$, and $\tilde{\varepsilon}(\mathbf{x})$, but C_D should be invoked to evaluate the length scale L, which is an input parameter of many combustion models, e.g. Eq. 4.

Thus, C_D should be either tuned or set arbitrarily in order to test any model of premixed turbulent combustion in RANS simulations of statistically stationary flames. Moreover, the inlet value of L requires tuning if an integral length scale was not measured.

4.2 Turbulent Schmidt number

In order to evaluate $D_{t,\infty}$ using Eq. 5, we have to know Sc_t, but available data on the turbulent Schmidt number are controversial. While it is set equal to 0.7 or 0.9 in a typical RANS study of a turbulent flame, very different numbers can be found in CFD literature. For instance, by reviewing RANS simulations of turbulent mixing in environmental processes, Tominaga and Stathopoulos [75] have concluded that "the optimum values for Sc_t are widely distributed in the range of 0.2–1.3". Bilger et al. [76] obtained $Sc_t = 0.35$ by experimentally studying reaction in a scalar mixing layer in grid-generated turbulence.

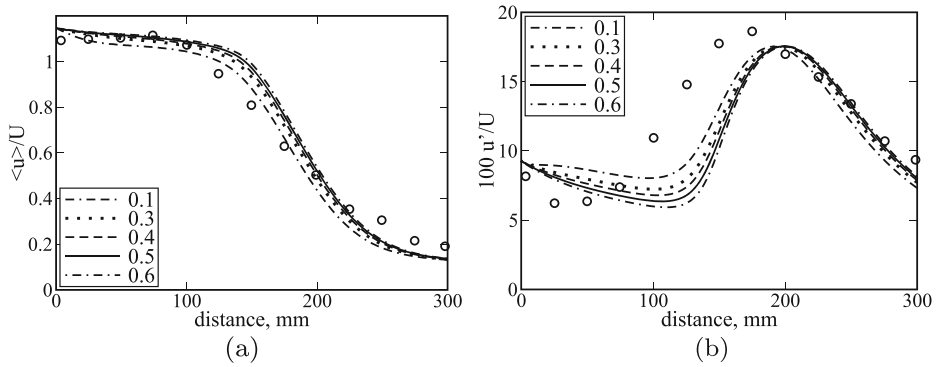

Fig. 3 Axial profiles of **a** the normalized mean axial velocity $\bar{u}/U$ and **b** the normalized rms velocity $100\sqrt{2\bar{k}/3}/U$ measured in the non-reacting cold case (*symbols*) and computed (*lines*) using the RNG $k-\varepsilon$ model with different values of C_D specified in legends

If we (i) apply Eqs. 5 and 15 to statistically stationary, homogeneous, isotropic turbulence and (ii) consider the diffusivity $D_{t,\infty}$ to be equal to $u'L_L$ [35], then, we arrive at $Sc_t = \sqrt{3/2}(C_\mu/C_D)(L/L_L)$. If a ratio of L/L_L is of unity order, then, this estimate of the turbulent Schmidt number can yield low values of Sc_t at low Reynolds numbers due to a significant increase in C_D when decreasing Re_t [70–74]. DNS data discussed by Yeung [73], see Fig. 3 in the cited paper, do show that a ratio of $\tilde{C}_0 = 4u'\bar{k}/(3\bar{\varepsilon}L_L)$ is substantially increased by Re_t and reaches 6.4 at the highest Reynolds number addressed in that DNS study. Using $D_{t,\infty} = u'L_L$ and Eq. 5, one can easily arrive at $Sc_t = 9C_\mu\tilde{C}_0/8$. Therefore, the largest Sc_t found in the discussed DNS is about 0.65, with significantly lower Sc_t being obtained at lower Re_t [73].

It is worth also noting that Sc_t used by the FSC model, which involves both Eqs. 5 and 9, is expected to be lower than Sc_t used by another, e.g. TFC, combustion model, that deals solely[3] with Eq. 5. Indeed, if Sc_t is tuned in RANS simulations of a flame and the simulations invoke either $D_t = D_{t,\infty}$ given by Eq. 5 or a lower (for the same Sc_t) diffusivity $D_t < D_{t,\infty}$ given by Eq. 9, with all other things being equal, then, the former tuned $Sc_{t,1}$ should be larger than the latter tuned $Sc_{t,2}$ in order for (i) the difference in $Sc_{t,1}$ and $Sc_{t,2}$ to counterbalance the difference in $D_{t,\infty}$ and D_t and (ii) the two simulations to agree with the same experimental data. For instance, in a single previous application of the FSC model to statistically stationary premixed turbulent flames, the best results were obtained with $Sc_t = 0.3$ [15].

4.3 Validation method

For the reasons discussed in the two previous subsections, both C_D in Eq. 15 and turbulent Schmidt number Sc_t in Eq. 5 were tuned in the present work. To reduce the influence of this

[3] A two-equation turbulence model invoked in a typical CFD study does not address the development of turbulent diffusivity, i.e. the time-dependent term on the RHS of Eq. 9, whereas this phenomenon is well established after the seminal work by Taylor [35]. Such a simplification is justified if the residence time is significantly larger than the Lagrangian time scale $\tau_L = L_L/u'$, as occurs in many non-reacting turbulent flows. However, the residence time and τ_L are of the same order in many premixed turbulent flames, where the development of turbulent diffusivity yields a well-pronounced effect, i.e. the linear dependence of mean flame brush thickness on distance from flame-holder, which is discussed in detail elsewhere [1, 11].

tuning on assessment of the TFC and FSC combustion models, the following method was applied.

For each set of measurements, a single reference case was selected and the aforementioned input parameters of turbulence and mixing models were tuned by simulating solely this case. When doing so, we tried (i) to minimize variations in the inlet value of L if an integral length scale of turbulence was measured, (ii) to start from the default value of $C_D = C_\mu^{3/4}$ and, then, to increase it bearing in mind the DNS data discussed in Section 4.1, and (iii) to start from $Sc_t = 0.7$ (or 0.3) for the TFC (FSC) model and to obtain tuned Schmidt number as close to this starting value as possible. The third requirement was set to be consistent (i) with previous applications of the TFC [7] or FSC [15] model and (ii) with reasoning discussed in the end of the previous subsection.

Five reference cases selected for the five sets of measurements addressed in the present work and the values of C_D and Sc_t that have been tuned by simulating these cases are summarized in Table 3. It requires a few comments.

First, because Moreau [17] did not report an integral length scale L, we kept $C_D = C_\mu^{3/4}$, but tested values of the inlet dissipation rate that had been used by other researchers to model the same experiment. The inlet values of $\tilde{\varepsilon}_b = 2.8 \cdot 10^6$ and $\tilde{\varepsilon}_u = 3.7 \cdot 10^4$ m^2/s^3 [44] or $\tilde{\varepsilon}_b = 6.1 \cdot 10^5$ and $\tilde{\varepsilon}_u = 6.85 \cdot 10^3$ m^2/s^3 [45] have been selected for the TFC or FSC model, respectively, in the present work.

Second, the TFC model is not applicable to the experiments by Pfadler et al. [22] and by Cohé et al. [23], because these flames were stabilized in very weak turbulence characterized by $u'/S_L = O(1)$ and, moreover, a low Re_t in the former measurements [22], whereas the model was developed by considering highly turbulent combustion. Because the TFC model substantially underestimates turbulent burning rate if $u' \leq S_L$, the model fails in yielding a statistically stationary flame under conditions of these experiments.

Third, the values of C_D reported in Table 3 are not in line with DNS data discussed in Section 4.2. One the one hand, the FSC C_D is sufficiently large for the flame investigated by Siewert [20] and characterized by a high Re_t, see Table 2. On the other hand, the FSC C_D appears to be too low for weakly turbulent flames investigated by Pfadler et al. [22] and by Cohé et al. [23]. It is worth noting, however, that we tuned neither C_D nor Sc_t when simulating experiments by Cohé et al. [23], because good agreement between measured and computed data was obtained at the first shot using the starting $Sc_t = 0.3$ and the default $C_D = C_\mu^{3/4}$. As far as the experiments by Pfadler et al. [22] are concerned, these flames are characterized not only by a low u'/S_L, but also by very low Reynolds numbers Re_t. Because the TFC model addresses flames that propagate in Kolmogorov turbulence associated with $\mathrm{Re}_t \gg 1$ and the FSC model is based on the TFC one, both models are not expected to

Table 3 Reference cases and tuned parameters

Flame	TFC		FSC		Ref.
	C_D	Sc_t	C_D	Sc_t	
ONERA, $\Phi = 0.8$	$C_\mu^{3/4}$	0.3	$C_\mu^{3/4}$	0.3	[17]
PSI, $\Phi = 0.5$, $P = 0.5$ MPa, $U = 40$ m/s, g350×g10	0.7	0.7	0.9	0.3	[20]
V-shaped, $\Phi = 0.7$	$C_\mu^{3/4}$	0.7	1.16	0.3	[19]
Erlangen-Bunsen, Flame C			$C_\mu^{3/4}$	0.3	[22]
Orléans-Bunsen, CH_4/air			$C_\mu^{3/4}$	0.3	[23]

be capable for predicting data measured by Pfadler et al. [22]. The goal of the present application of the FSC model to simulations of these experiments consists of gaining an insight into the model limitations, rather than quantitatively validating it.

Fourth, the axial profiles of the Reynolds-averaged combustion progress variable measured in the reference case selected for the PSI experiments [20] can be well predicted using various combinations of Sc_t and C_D, as shown in Fig. 4. The combinations reported in Table 3 were selected in order to have Sc_t equal to its starting values. Moreover, the reference flame angle measured by Dinkelacker and Hölzler [19] was well predicted using the FSC model with different combinations of Sc_t and C_D. In the following, we will report results obtained using $Sc_t = 0.3$.

Thus, the same value of the turbulent Schmidt number Sc_t was selected for the FSC model in all five reference cases and the same value of $Sc_t = 0.3$ was earlier set to simulate confined, preheated, lean propane-air flames stabilized behind a bluff body [15]. Accordingly, all five sets of flames addressed in the present work and the flames investigated in Ref. [15] were simulated using the FSC model with the same constant $A = 0.5$ and the same $Sc_t = 0.3$ in all six cases, whereas the inlet dissipation rate or C_D was tuned by computing a single reference flame in each case.

To conclude this section, it is worth showing the influence of Sc_t, the inlet $\bar{\varepsilon}$, and C_D on computed results. To do so, we will restrict ourselves to a single reference case from Table 3, i.e. the reference case relevant to the experiments by Moreau [17]. In other studied cases, trends were basically similar.

Figure 5 shows that an increase in Sc_t results in decreasing the mean flame brush thickness or increasing the slope of computed transverse profiles of $\tilde{c}(y)$. These trends are expected, because the turbulent diffusivity $D_{t,\infty}$ is inversely proportional to Sc_t. The transverse coordinate of the mean flame surface ($\bar{c} = 0.5$ or $\tilde{c} = 0.21$ in this particular case) yielded by the TFC model varies weakly when Sc_t is increased from 0.3 to 0.9, see Fig. 5a, thus, indicating weak sensitivity of the computed turbulent burning velocity to the turbulent Schmidt number. The transverse coordinate y_f of $\tilde{c}(y) = 0.21$, computed using the FSC model, is lower for a lower Sc_t, thus, indicating a decrease in U_t when decreasing Sc_t. The point is that $f_2(\theta_{fd})$ on the RHS of Eq. 10 is a monotonously increasing function of the normalized flame-development time, while a decrease in Sc_t results in increasing $D_{t,\infty}$ and $\tau_t = D_{t,\infty}/u'^2$, thus decreasing θ_{fd}, f_2, and, hence, U_t. The magnitude of the effect

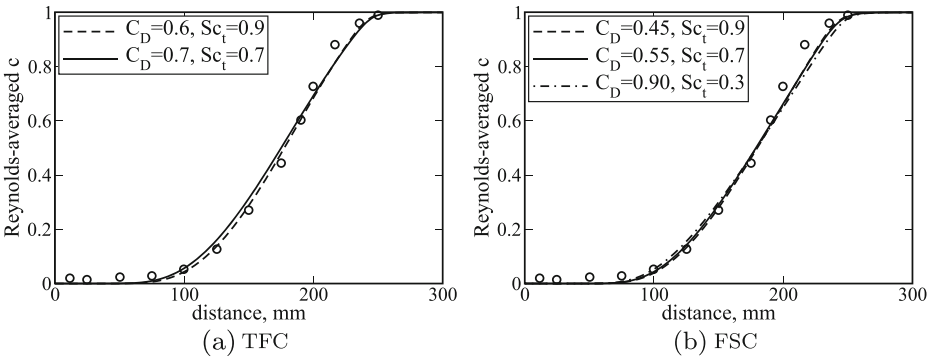

Fig. 4 Axial profiles of the Reynolds-averaged combustion progress variable computed (*lines*) using the TFC **a** and FSC **b** combustion models and various Sc_t and C_D specified in legends. *Symbols* show the mean intensity of OH PLIF signal obtained by Siewert [20] from the PSI flame in the reference case

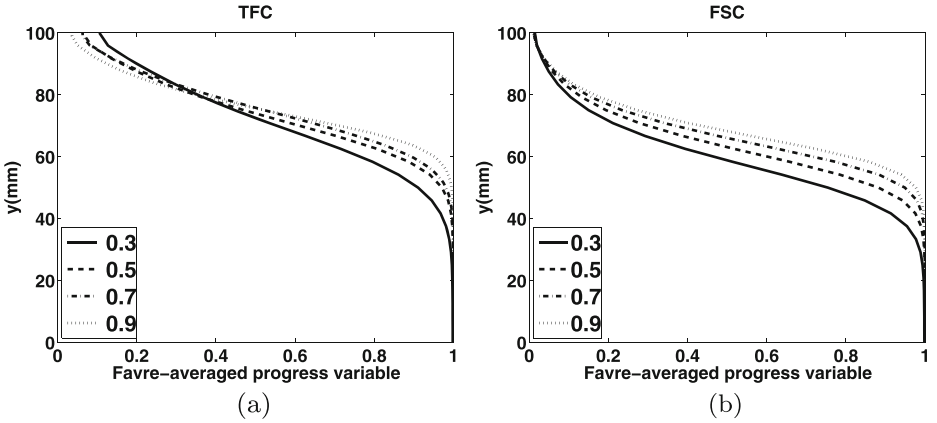

Fig. 5 Effect of variations in the turbulent Schmidt number, which is specified in legends, on transverse profiles of the Favre-averaged combustion progress variable $\tilde{c}(y)$, computed using **a** TFC or **b** FSC model under conditions of the experiments by Moreau [17]. $\Phi = 0.8$, $x = 522$ mm

is sufficiently small. For instance, the difference in y_f computed using $Sc_t = 0.3$ and 0.5, cf. solid and dashed curves, respectively, is less than 5 % of the flame propagation distance $y_f(x) - y_f(0)$, where $y_f(0) = 20$ mm.

Figure 6 shows that an increase in the inlet ε results in decreasing the mean flame brush thickness (or increasing the slope of $\tilde{c}(y)$-curves) and decreasing the transverse coordinate of the mean flame surface, i.e. decreasing turbulent burning velocity. The two effects are controlled by (i) a decrease in the diffusivity $D_{t,\infty}$ when increasing $\tilde{\varepsilon}$, see Eq. 5, and (ii) by a decrease in the length scale L when increasing $\tilde{\varepsilon}$, see Eq. 15, respectively. These effects are less (more) pronounced when using FSC (TFC) model. The point is that an increase in the dissipation rate results not only in decreasing $U_{t,ISF}$ and $D_{t,\infty}$, see Eqs. 4 and 5, respectively, but also in decreasing the time scale $\tau_t = D_{t,\infty}/u'^2$. The decrease in τ_t results

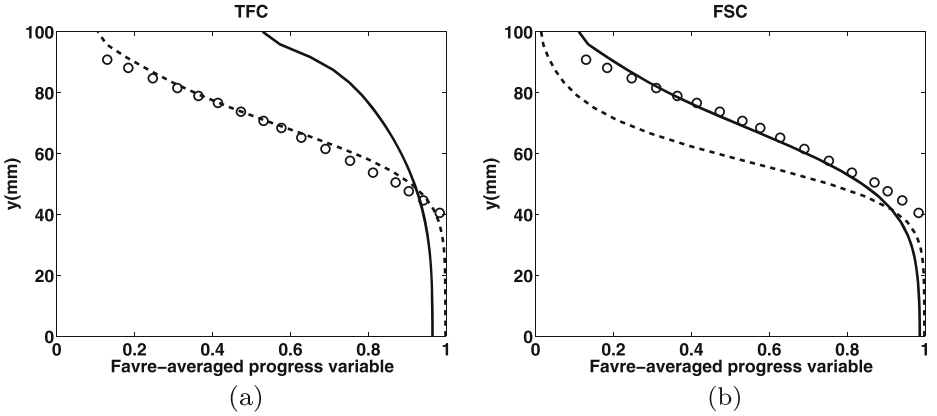

Fig. 6 Effect of variations in the inlet dissipation rate on transverse profiles of the Favre-averaged combustion progress variable $\tilde{c}(y)$, computed using **a** TFC or **b** FSC model under conditions of the experiments by Moreau [17]. *Dashed* and *solid curves* were obtained by setting $\tilde{\varepsilon}_b = 2.8 \cdot 10^6$ m^2/s^3, $\tilde{\varepsilon}_u = 3.7 \cdot 10^4$ m^2/s^3 [44] and $\tilde{\varepsilon}_b = 6.1 \cdot 10^5$ m^2/s^3, $\tilde{\varepsilon}_u = 6.85 \cdot 10^3$ m^2/s^3 [45], respectively. *Symbols* show experimental data by Moreau [17]. $\Phi = 0.8$, $Sc_t = 0.3$, $x = 522$ mm

in increasing θ_{fd} and the functions $f_k(\theta_{fd})$ on the RHSs of Eqs. 9 and 10. It is worth stressing that the significant sensitivity of computed results to the inlet dissipation rate is relevant to our study of the ONERA flames [17] only. Because an integral length scale L was measured in other experiments addressed in the present work, we tuned C_D when simulating them.

Figure 7 shows that an increase in C_D results in decreasing the mean flame brush thickness (or increasing the slope of the computed $\tilde{c}(y)$-curves) due to a decrease in $D_{t,\infty}$, see Eqs. 5 and 15. Moreover, shorter distances y_f associated with $\tilde{c}(y) = 0.21$ (or $\bar{c} = 0.5$) and, hence, lower burning rates were obtained when increasing C_D. This effect is controlled by a decrease in u' when increasing the dissipation rate, with all other things being equal. For the FSC model, the latter effect is less pronounced, i.e. $(y_f(C_D = 0.3) - y_f(C_D = 0.9)) < 0.1(y_f(x) - y_f(0))$, cf. solid and dotted-dashed curves in Fig. 7b, because the increase in C_D results in increasing $f_k(\theta_{fd})$ on the RHSs of Eqs. 9 and 10 due to a decrease in $\tau_t \propto \tilde{k}/\tilde{\varepsilon}$. The influence of C_D on $U_{t,ISF}$ due to variations in the length scale L, see Eq. 4, is weakly pronounced. Indeed, L evaluated locally using Eq. 15 depends weakly on C_D, because an increase in the local $\tilde{\varepsilon}$ due to an increase in the inlet $\tilde{\varepsilon}$ is counterbalanced by the increase in C_D that controls the aforementioned increase in the inlet dissipation rate.

5 Test Results and Discussion

After tuning Sc_t and C_D (or the inlet $\bar{\varepsilon}$ for the ONERA flames) by studying a single reference case, exactly the same Sc_t and C_D (or the inlet $\bar{\varepsilon}$) were set to simulate all other cases pertaining to the same set of measurements. No further tuning was applied at this stage of simulations and the same value $A = 0.5$ of a single (if $P_q = 0$ or $\varepsilon_q \to \infty$) constant of the TFC or FSC model was used in all cases.

5.1 ONERA experiments

Shown in Fig. 8 are results of testing the TFC (dashed lines) and FSC (solid and dotted-dashed lines) models against experimental data by Moreau [17], obtained for all equivalence

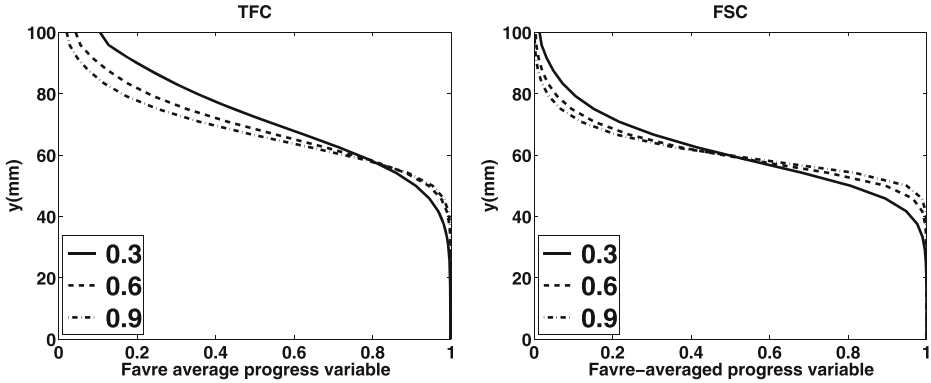

Fig. 7 Effect of variations in C_D, which is specified in legends, on transverse profiles of the Favre-averaged combustion progress variable $\tilde{c}(y)$, computed using **a** TFC or **b** FSC model under conditions of the experiments by Moreau [17]. $\Phi = 0.8$, $Sc_t = 0.3$, $x = 522$ mm

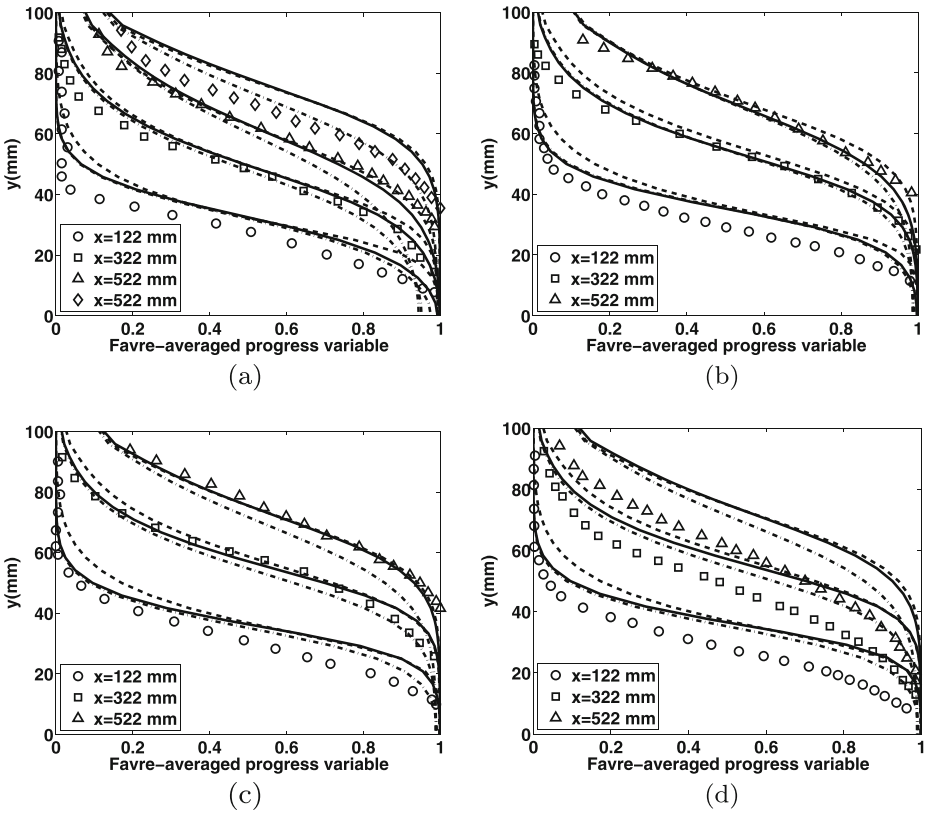

Fig. 8 Transverse profiles of the Favre-averaged combustion progress variable $\tilde{c}(y)$, computed using the TFC model (*dashed lines*), FSC model (*solid lines*), and FSC model with $Q_L = 0$ (*dotted-dashed lines*). *Symbols* show experimental data obtained by Moreau [17] at various distances x from the inlet (the splitter edge), specified in legends. **a** *Circles*, *squares*, and *triangles* show data obtained from flames with $\Phi = 0.62$, while *diamonds* correspond to the stoichiometric flame. **b** $\Phi = 0.80$, **c** *Circles*, *squares*, and *triangles* show data obtained from flames with $\Phi = 0.83$, 0.85, and 0.87, respectively. **d** $\Phi = 1.24$

ratios investigated in the cited paper. All in all, both the TFC and FSC models yield sufficiently good agreement with the experimental data, with the performance of the latter model being slightly better. Both models are capable for reasonably well predicting the influence of the equivalence ratio on the mean flame structure and burning rate under conditions of the experiments by Moreau [17], at least for lean and stoichiometric mixtures. In a single rich case of $\Phi = 1.24$, see Fig. 8d, the computed $\tilde{c}(y)$-profiles are shifted toward the cold wall when compared to the measured data, i.e. the models moderately overpredict burning rate in this particular case.

More specifically, the FSC model well predicts the mean flame brush thickness, i.e. the maximum slope of $\tilde{c}(y)$-curves, in all cases with exception of a single case of $x = 122$ mm and $\Phi = 0.83$, where the maximum slope is overestimated, see Fig. 8c. The mean flame position y_f associated with $\tilde{c}(y_f) = 0.5$, i.e. $\tilde{c} = 0.20 - 0.24$ depending on the density ratio, and, hence, the burning rate are well predicted in most cases, but they are notably overpredicted in the cases of $x = 122$ mm and $\Phi = 0.62$, see Fig. 8a, $x = 122$ mm and $\Phi = 0.80$, see Fig. 8b, and all distances and $\Phi = 1.24$, see Fig. 8d. The maximum

difference Δy_f between the measured and computed y_f is about 15 mm and obtained in the case of $x = 522$ mm and $\Phi = 1.24$, see Fig. 8d. The relative error $\Delta y_f/(y_f(x) - y(0))$ is about 25 % in this worst case. When compared to the FSC model, the TFC model (dashed lines) overestimates y_f and burning rate in the cases of $x = 122$, 322 mm and $\Phi = 0.80$, see Fig. 8b, $x = 122$ mm and $\Phi = 0.83$, see Fig. 8c, $x = 122$ mm and $\Phi = 1.24$, see Fig. 8d. In a single case of $x = 122$ mm and $\Phi = 0.83$, see Fig. 8c, the TFC model predicts the maximum slope $|\partial\tilde{c}/\partial y|$ better than the FSC model.

While results simulated using the TFC and FSC models are sufficiently close to one another in many cases, it is worth remembering that the latter results have been obtained by setting lower inlet $\tilde{\varepsilon}$. The decrease in the dissipation rate results in (i) increasing turbulent diffusivity, see Eq. 5, thus, counterbalancing $f_1(\theta_{fd}) \leq 1$ on the RHS of Eq. 9, and (ii) increasing L, $\tilde{k}$, u', and, hence, $U_{t,ISF}$, see Eq. 4, thus, counterbalancing $f_2(\theta_{fd}) \leq 1$ on the RHS of Eq. 10. Accordingly, the difference in the inlet $\tilde{\varepsilon}$ has allowed us to obtain close results using two different models.

Comparison of results shown in solid and dotted-dashed lines indicates that the source term Q_L, see Eq. 2, plays a role by making $\tilde{c}$ closer to unity at the tail of flame brush. However, for these highly turbulent flames, the effect is mainly pronounced at large $\tilde{c}$. It is worth noting that if $Q_L = 0$, then, Eqs. 1–2 have a trivial solution of $\tilde{c} = 0$, which can attract CFD solution due to numerical errors. The use of Eq. 11 eliminates the trivial solution.

Finally, it is worth noting that results computed by us using the TFC model in the case of $\Phi = 0.8$ differ from results published earlier by Zimont et al. [44, 45], because a finite tuned $\dot{s}_q$ was set in the cited papers, thus, making term $(1 - P_q)$ on the RHS of Eq. 8 lower than unity.

5.2 PSI experiments

Results of testing the TFC and FSC models against the experimental data by Siewert et al. [20] are summarized in Fig. 9.

Figure 9 indicates that results computed using the TFC and FSC models are close to one another. This observation was confirmed by setting the same C_D and Sc_t for the two models (not shown). The point is that the studied flames are long and the residence time of a fluid particle in the combustion chamber is substantially larger than the turbulence time scale. Accordingly, the time-dependent terms on the RHSs of Eqs. 9 and 10 are close to unity in the largest part of the flame brush, whereas the source term Q_L plays a minor role in so-intense turbulence. Therefore, the differences between the TFC and FSC models are minor in this particular case.

In the majority of the studied cases,[4] the two models predict the measured data well. In particular, the simulations predict (i) a weak influence of pressure on X_{MP} and ΔX_{MP}, see Fig. 9a, (ii) a weak increase in X_{MP} and ΔX_{MP} by the bulk velocity U, see Fig. 9c, and (iii) variations in X_{MP} with the grids, with a single exception of g365×g10 (note that mean and turbulent cold flows generated by this grid differed from mean and turbulent flows generated by all other grids, as discussed in detail by Siewert [20]).

Mean flame positions X_{MP} computed using both models quantitatively agree with the experimental data, i.e. differences between measured and computed results are less than the experimental errors reported by Siewert [20], in all cases (various grids and bulk flow

[4]Recent LESs [47, 48] of the PSI flames were solely restricted to the bulk velocity $U = 40$ m/s, grid g350×g10, and the equivalence ratio $\Phi = 0.5$.

velocities) characterized by $F = 0.5$ with a single exception of grid g365×g10. Differences between measured and computed flame brush thicknesses are larger than the experimental errors also for grid g350×g30, but it is worth remembering that different methods were used to evaluate the thickness in the measurements and simulations, see Section 3.2.1.

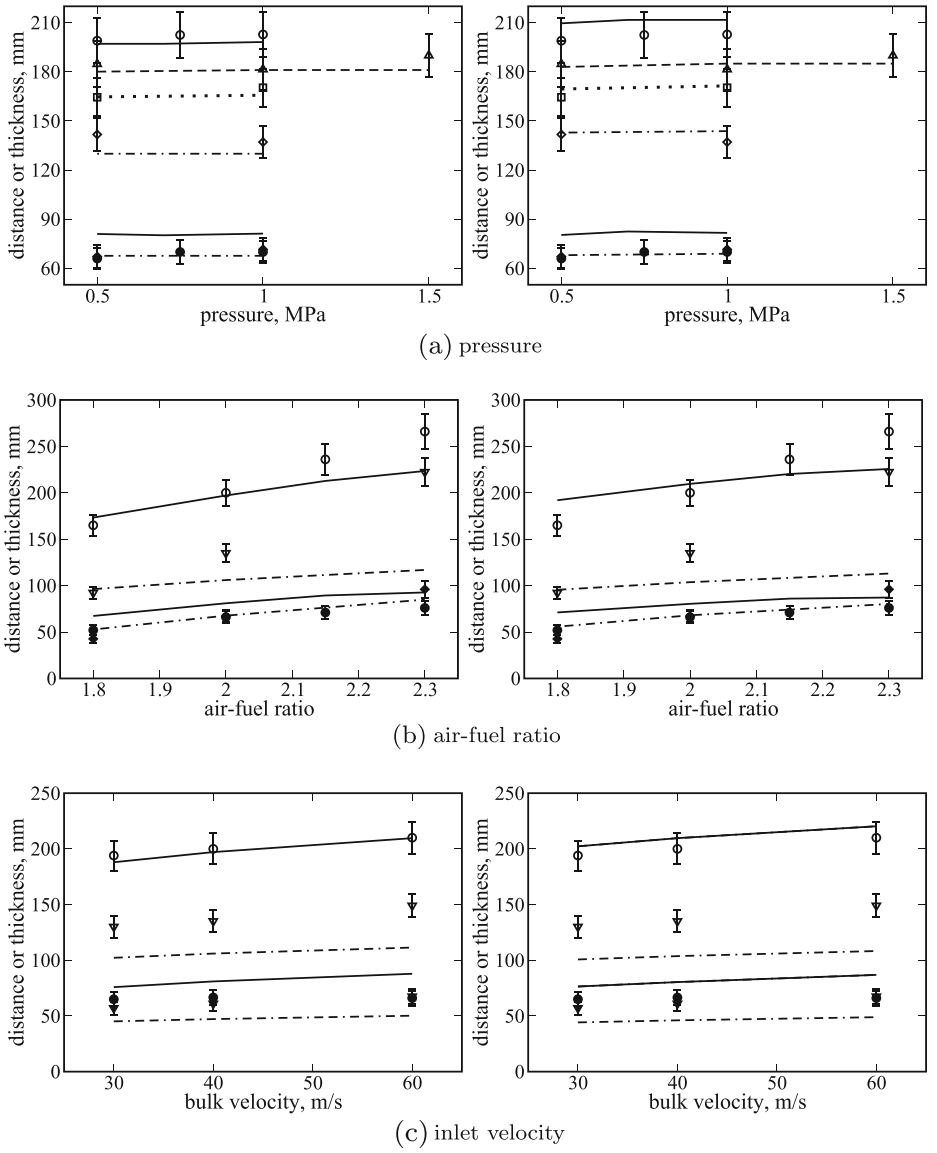

Fig. 9 The mean centerline flame position X_{MP} (*open symbols*) and the mean centerline flame brush thickness ΔX_{MP} (*filled symbols*) vs. **a** pressure P, **b** air-fuel ratio $1/\Phi$, and **c** inlet bulk velocity U. *Symbols* show experimental data by Siewert [20]. Results computed using TFC and FSC models are shown in left and right columns, respectively. *Circles* and *solid lines*—g350×g30, *triangles-up* and *dashed lines*—g350×g10, *squares* and *dotted lines*—g450×g10, *diamonds* and *dotted-dashed lines*—g465×g10, *triangles-down* and *double-dashed-dotted lines*—g365×g10

Substantial disagreement between measured and computed results is observed in Fig. 9b, which shows that the influence of the equivalence ratio on X_{MP} is substantially underpredicted. This result is surprising, because the capabilities of the TFC or FSC model for predicting the influence of mixture composition on turbulent burning rate are well documented, as reviewed elsewhere [1, 11]. Moreover, the authors of the considered measurements concluded that "the comparison of the experimental turbulent flame speed data with" Eq. 4 showed "satisfactory agreement" [21]. Furthermore, substitution of $S_L(\Phi = 0.56) = 0.325$ m/s and $S_L(\Phi = 0.43) = 0.129$ m/s into Eq. 4 shows that the turbulent burning velocity should be higher by a factor of 1.6 for the former mixture, whereas a significantly weaker effect is observed in Fig. 9.

The fact that the computed X_{MP} depends weaker on the equivalence ratio when compared to $U_{t,ISF}(\Phi)$ yielded by Eq. 4 implies that an increase in S_L by Φ is counteracted by variations in the turbulence characteristics computed when varying Φ. Indeed, Fig. 10 shows that a ratio u'/U of the local rms velocity to the inlet bulk velocity U, evaluated along iso-lines $\tilde{c}(x,r) = 0.5$ and 0.7, is substantially larger for the leanest ($\Phi = 0.43$) flame. This difference in the local u' counterbalances a decrease in the Damköhler number when decreasing Φ. As a result, the computed local values of $U_{t,ISF}$ are sufficiently close to one another, especially along the iso-line $\tilde{c}(x,r) = 0.7$.

The aforementioned difference in the local u' computed for $\Phi = 0.56$ and 0.43 is associated with the fact that the leaner flame is characterized by a lower density ratio and by heavier combustion products, which resist to the reactant jet stronger, thus, promoting turbulence generation when compared to richer ($\Phi = 0.56$) products. However, as reviewed elsewhere [34], turbulence models developed for constant-density flows do not allow for certain effects that are well pronounced in flames. For instance, term $-\overline{\mathbf{u}'' \cdot \nabla p}$ can result in significant turbulence production in flames, with the effect being increased by the density ratio, thus, counterbalancing the aforementioned decrease in the local u' with increasing Φ. A target-directed study of such an effect and other relevant phenomena is impeded by the fact that a predictive model of the influence of combustion on turbulence has not yet been developed.

A weak effect of Φ on X_{MP}, shown in Fig. 9, is not specific to the used turbulence model and similar results were obtained invoking other turbulence models implemented into Fluent, see Fig. 11. To the contrary, the measured dependence of X_{MP} on Φ was better predicted, cf. filled and open circles, when spatially uniform u' and L were set by switching off a turbulence model. This observation is in line with the fact that the PSI "measurements have shown that the average flame front surface closely corresponds to a u' isosurface"

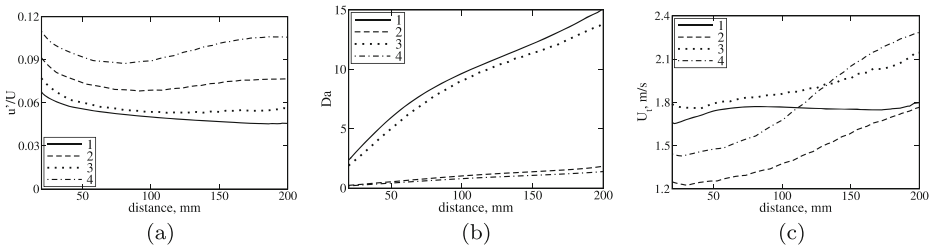

Fig. 10 Variations of **a** normalized rms turbulent velocity $\sqrt{2\tilde{k}/3}/U$, **b** Damköhler number Da, and **c** filly-developed turbulent flame speed $U_{t,ISF}$ given by Eq. 4 along iso-lines $\tilde{c}(x,r) = 0.5$ (curves 1 and 2) and $\tilde{c}(x,r) = 0.7$ (curves 3 and 4), computed for $\Phi = 0.56$ (curves 1 and 3) and $\Phi = 0.43$ (curves 2 and 4) using the TFC model

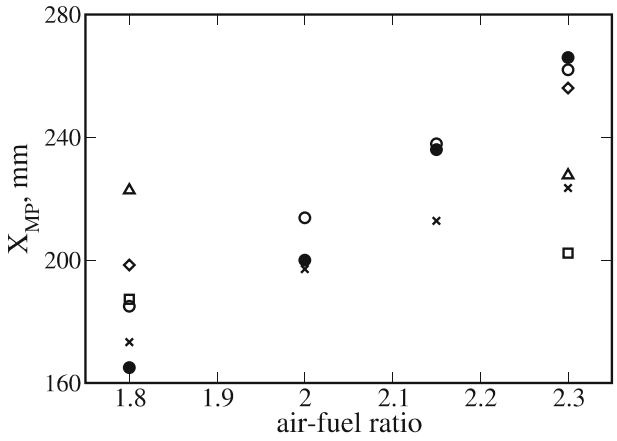

Fig. 11 The mean centerline flame position X_{MP} vs. the air-fuel ratio $1/\Phi$. *Filled circles* show experimental data by Siewert [20] obtained for grid 350×g30. Other symbols show results computed using various turbulence models implemented into Fluent; RNG $k-\varepsilon$ model (*crosses*), standard $k-\varepsilon$ model (*squares*), realizable $k-\varepsilon$ model (*diamonds*), Reynolds-stress model (*triangles*), and frozen turbulence (*open circles*)

[56], which is also a L isosurface, see Fig. 2 in the cited paper. It is worth noting that, by analyzing a large set of earlier experimental data obtained from various premixed turbulent flames [9] and by performing target-directed measurements [77], Prudnikov [9] argued that bulk flame characteristics such as burning velocity and mean thickness are controlled by characteristics of incoming cold-flow turbulence, rather than local turbulence characteristics within the flame brush.

When the present numerical study of the experiments by Siewert et al. [20] was completed, we found more experimental data obtained from the PSI flames in the case of $U = 40$ m/s, $\Phi = 0.5$, and g350×g10. These data were reported in a form of the radial profiles of both the Reynolds- and Favre-averaged combustion progress variables in Ref. [47]. Note that the profiles of $\bar{c}(r)$ were measured, whereas the mass-weighted profiles of $\tilde{c}(r)$ were calculated [47] using the BML Eqs. 6 and 14. To test the TFC and FSC models against these data, which were not reported in the thesis [20], we did not run new simulations, but restricted ourselves to processing results computed earlier in the same case ($U = 40$ m/s, $\Phi = 0.5$, and g350×g10). Figure 12 shows computed Favre profiles of $\tilde{c}(r)$, see solid lines, as well as the counterpart profiles calculated by processing raw experimental data, see symbols. Only data obtained using the TFC model for $P = 0.5$ MPa are plotted, because the TFC and FSC models yield similar $\tilde{c}(r)$ under conditions of the PSI measurements and both the numerical results and experimental data exhibit very weak sensitivity to the pressure.

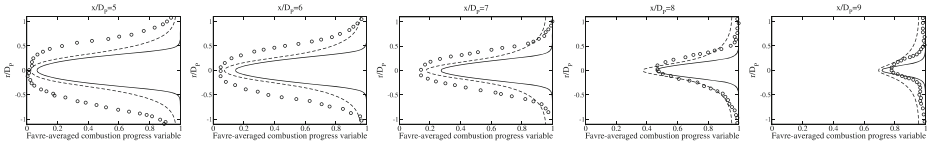

Fig. 12 Radial profiles of the Favre-averaged combustion progress variable, measured (*symbols*) and computed (*lines*) at different distances x/D_P from the inlet, where D_P is the diameter of the inlet pipe. *Solid and dashed* curves were computed using the TFC model with $\dot{s}_q \to \infty$ and $\dot{s}_q = 3.5/\tau_c$, respectively

On the one hand, agreement (or disagreement) between the present RANS results shown in solid curves and the experimental data shown in symbols is very similar to agreement (or disagreement) between the best LES results obtained earlier by Duwig et al. [47] and the same measured data, see Fig. 12 in the cited paper. This fact is encouraging, because (i) LES is commonly considered to be a superior numerical tool for simulating flames similar to PSI ones, and (ii) the present RANS results plotted in Fig. 12 were obtained before we found the experimental profiles of $\bar{c}(r)$.

On the other hand, the disagreement between the experimental data and the present RANS (or earlier LES) results is substantial. The simulations either underpredict the radial growth of the mean flame brush due to turbulent diffusion or overpredict turbulent flame speed in the radial direction. This difference between the measured and computed data could in part be attributed to limitations of the used turbulence model, as discussed above. Moreover, it could be attributed to eventual local combustion quenching. For instance, dashed curves obtained using Eqs. 7 and 8 with $\dot{s}_q = 3.5/\tau_c$ agree with the experimental data substantially better. Further study of this issue is required.

5.3 Erlangen V-shaped flames

Figures 13 and 14 report results of testing the TFC and FSC models against experimental data obtained by Dinkelacker and Hölzler [19] from Erlangen Bunsen flames. 2D images of the Reynolds-averaged combustion progress variable $\bar{c}$ computed using the TFC (the first raw in Fig. 13) and FSC (the second raw) models agree well with the experimental images (the third raw) in the leanest flames characterized by $\Phi = 0.5$ and $u'/S_L = 5.4$ (left column) or $\Phi = 0.58$ and $u'/S_L = 2.6$ (middle column).

In the richest case characterized by $\Phi = 0.7$ and $u'/S_L = 1.3$, the FSC model appears to underpredict the mean flame brush thickness δ_t, cf. images (b) and (c) in the right column. Because such an effect is not obtained using the TFC model, see upper image in the right column, a smaller flame brush thickness yielded by the FSC model in the richest case is attributed to the laminar-like source term Q_L, which vanishes within the framework of the TFC model. This explanation was also confirmed by running the FSC model with $Q_L = 0$ (not shown). In the leaner flame with $\Phi = 0.58$, the role played by Q_L is reduced due to a higher u'/S_L and the FSC model well predicts δ_t. Thus, results reported in Fig. 13 imply that the simplest linear combination of the gradient source term $\rho_u U_t |\nabla \tilde{c}|$ and the laminar-like source term Q_L on the RHS of Eq. 12 oversimplifies the problem and a more sophisticated combination of these two limit source terms should be developed in order to improve capabilities of the FSC model for predicting turbulent flames associated with $u'/S_L = O(1)$.

The fact that the TFC model predicts the thickness of the richest flame better than the FSC model is not sufficient to claim that the former model shows better performance in this particular case. For instance, Fig. 14 indicates that the FSC model well predicts the measured flame half angle φ, whereas the TFC model overestimates it.

It is also worth noting that the TFC model was already validated against the experimental data by Dinkelacker and Hölzler [19] in earlier studies [19, 46, 49]. Results reported in the cited papers look similar to Fig. 13 at a first glance, but the shape of the richest flame varies from slightly convex, see Fig. 4 in Ref. [19] or Fig. 2 in Ref. [49], to slightly concave, see Fig. 5 in Ref. [46]. Moreover, the TFC model slightly underestimated the measured φ in the simulations by Dinkelacker and Hölzler [19], see Fig. 5b in the cited paper, whereas neither Ghirelli [46], nor Moreau [49] reported computed half angles. The cause of this difference is unclear, but different Sc_t and C_D were set in these simulations.

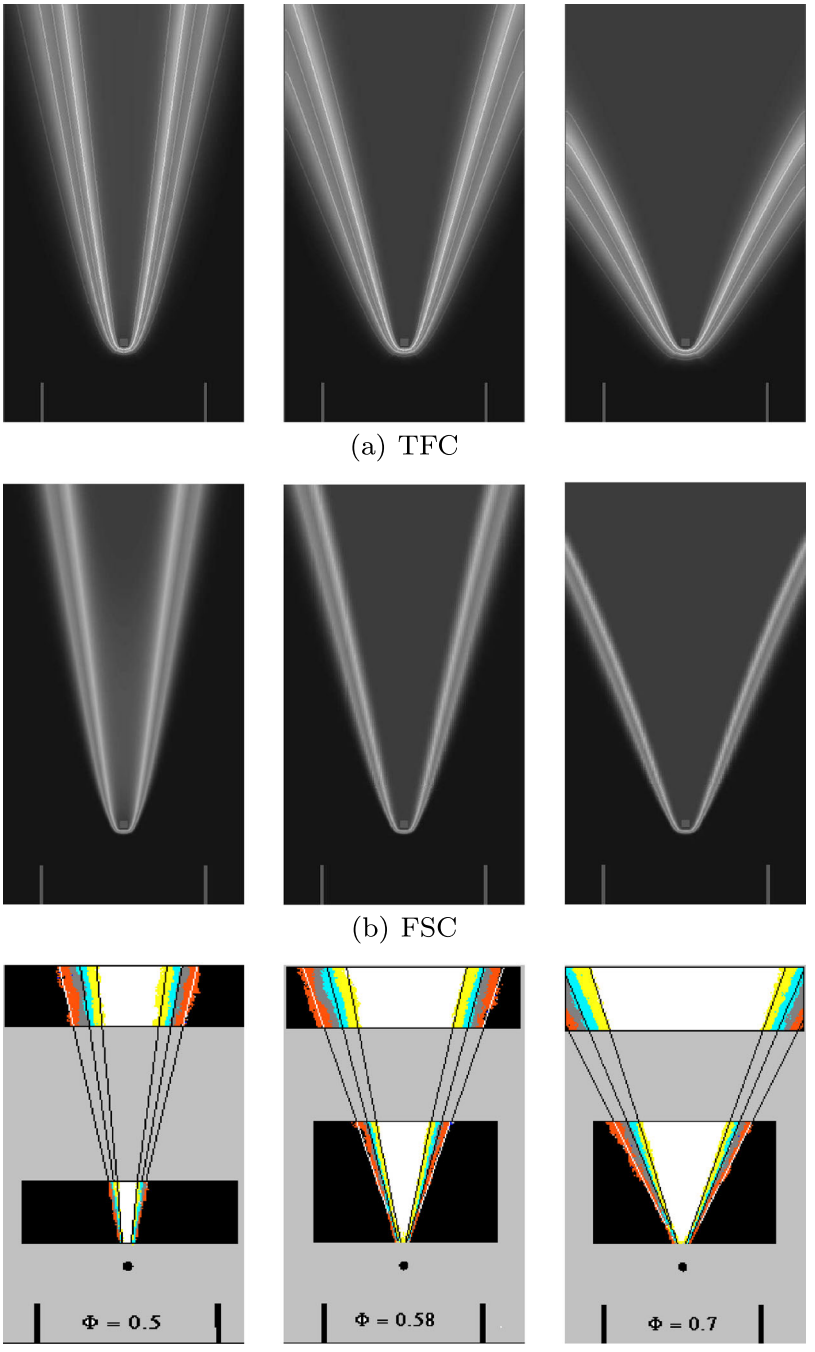

Fig. 13 2D fields of the Reynolds-averaged combustion progress variable $\tilde{c}$ computed using **a** the TFC model or **b** the FSC model and **c** measured by Dinkelacker and Hölzler [19]. Left, middle, and right columns show results obtained from flames with $\Phi = 0.5$, 0.58, and 0.7, respectively

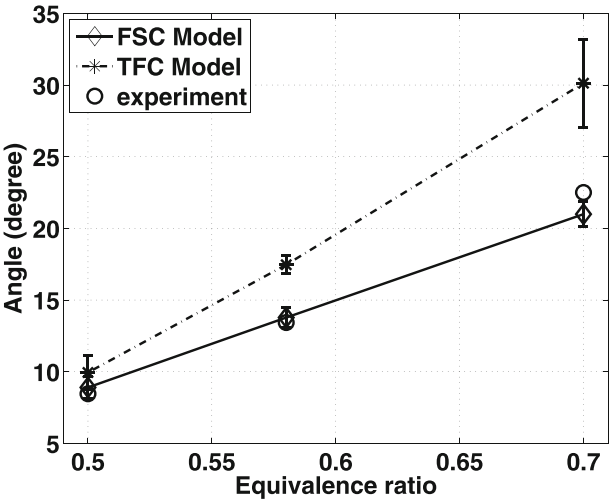

Fig. 14 The flame half angle φ vs. equivalence ratio Φ. Error bars show variations in the computed φ in the range of x =15–45 mm

5.4 Erlangen Bunsen flames

Figure 15 shows that although the FSC model predicts (a) a substantial decrease in the flame height with the equivalence ratio and (b) a weak increase in the flame height with the mass flow rate under conditions of the experiments by Pfadler et al. [22], there are quantitative differences between the measured and computed data. First, the FSC model underestimates the mean flame brush thickness in all investigated cases, with the effect being increased by the equivalence ratio, cf. dotted-dashed and dashed curves in Fig. 15a. This limitation of the model can be attributed to the oversimplified linear combination of the gradient source term $\rho_u U_t |\nabla \tilde{c}|$ and the laminar-like source term Q_L, as discussed in the previous subsection.

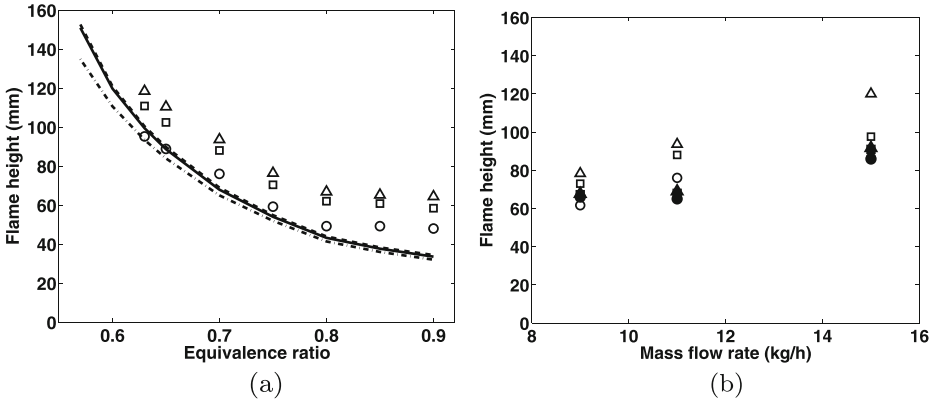

Fig. 15 Axial heights of various iso-scalar surfaces vs. **a** the equivalence ratio Φ in the case of $\dot{m} = 12$ kg/h and **b** the mass flow rate $\dot{m}$ in the case of $\Phi = 0.7$. *Open symbols* and **a** *lines* or **b** *filled symbols* show experimental data by Pfadler et al. [22] and results computed using the FSC model, respectively. $\bar{c} = 0.1$—*circles* and *dotted-dashed line*, $\bar{c} = 0.5$—*squares* and *solid line*, $\bar{c} = 0.9$—*triangles* and *dashed line*

When the equivalence ratio is decreased, the role played by Q_L is reduced due to an increase in u'/S_L and computed δ_t is increased.

Second, the FSC model overestimates burning rate (yields lower flame height) in the richest flames ($\Phi = 0.85$ and 0.9), cf. curves with symbols in Fig. 15a. Such a quantitative difference is not surprising, because these flames are characterized by too low u'/S_L, which is substantially less than unity, and too low $\mathrm{Re}_t = 25$. Nevertheless, the model quantitatively predicts the height of the leading edge ($\bar{c} = 0.1$) of the mean flame brush in the leanest cases ($\Phi = 0.63$ and 0.65) characterized by $u' > S_L$. This result is surprising and encouraging bearing in mind the low Re_t of the flames investigated by Pfadler et al. [22].

5.5 Orléans Bunsen flames

Axial profiles of the Reynolds-averaged combustion progress variable, computed using the FSC model for different mole fractions of CO_2 in the fuel, are compared with the experimental data by Cohé et al. [23] in Fig. 16. In the largest parts of the flame brushes, good agreement was obtained at the first shot. In particular, the model predicts an increase in y_f associated with $\bar{c}(y_f) = 0.5$ due to addition of CO_2 to methane. The mean flame

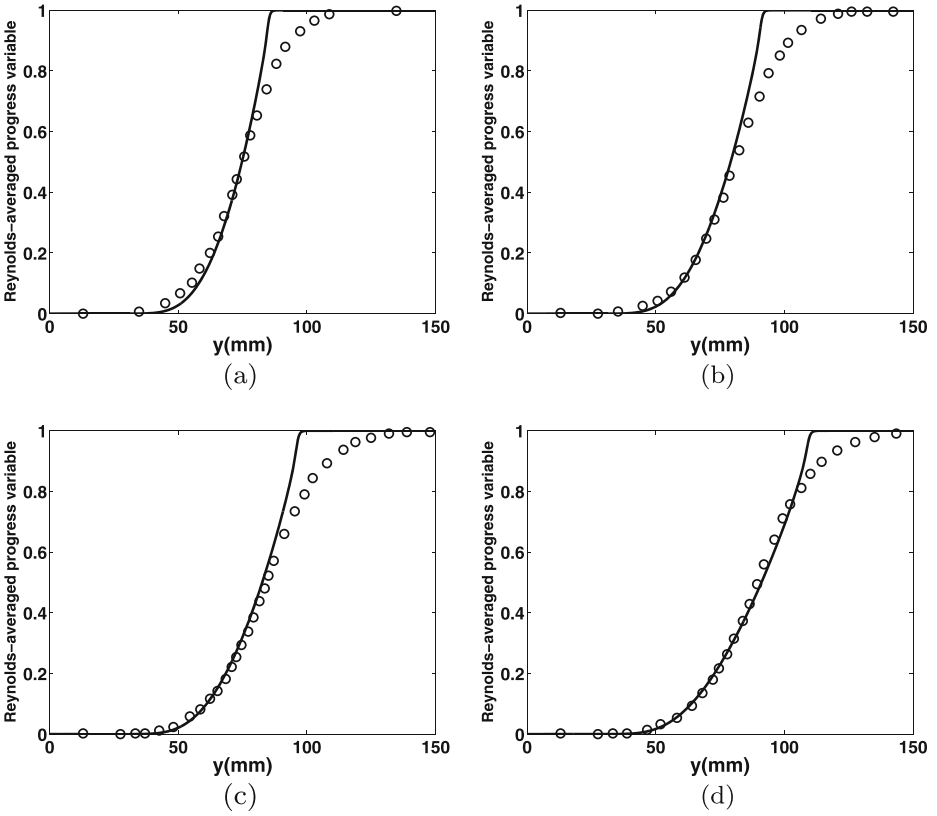

Fig. 16 Axial profiles of the Reynolds-averaged combustion progress variable $\bar{c}$, computed (*lines*) using the FSC model and obtained (*symbols*) by Cohé et al. [23] from Bunsen flames at various mole fractions of CO_2 in the fuel. **a** CH_4, **b** $0.1CO_2$+$0.9CH_4$, **c** $0.2CO_2$+$0.8CH_4$, **d** $0.35CO_2$+$0.65CH_4$

brush thickness, i.e. the maximum slope $\max\{\nabla\bar{c}\}$ of the centerline $\bar{c}$-profile, is also well predicted, including a decrease in the slope with addition of CO_2. However, the model overpredicts $\bar{c}$ at the trailing parts of the flame brushes, thus, implying that the simplest linear combination of the two source terms, $U_t|\nabla\tilde{c}|$ and Q_L, overpredicts burning rate in weakly turbulent premixed flames at large $\bar{c}$, where the simulated burning rate is mainly controlled by Q_L.

It is encouraging that Fig. 16a indicates substantially better agreement between measured and computed data when compared to results obtained in a recent LES modeling study [51] of a similar experiment by Halter et al. [50], cf. the present Fig. 16a with Figs. 8a and 8c in Ref. [51].

6 Conclusions

Turbulent Flame Closure (TFC) and Flame Speed Closure (FSC) models of the influence of turbulence on premixed combustion were tested in RANS simulations of five sets of experiments with (i) highly turbulent, oblique, confined ONERA flames under elevated temperatures, (ii) highly turbulent, conical, confined PSI flames under elevated temperatures and pressures, (iii) open V-shaped flames, and weakly turbulent Bunsen (iv) Erlangen and (v) Orléans flames under the room conditions. Besides flame geometry, pressure, and initial temperature, bulk flow velocities, turbulence characteristics, and mixture compositions were different in these five sets of flames, with the equivalence ratio being varied in each set.

The TFC and FSC combustion models yielded similar results when simulating the PSI flames, but the FSC model showed better performance in predicting burning rate for four other sets of flames, especially for weakly turbulent Erlangen and Orléans Bunsen flames, which could not be simulated using the TFC model developed for highly turbulent flows. All in all, results computed using the FSC model with the same standard value $A = 0.5$ of a single model constant agree reasonably well with the majority of the experimental data utilized to test the model, but the following two exceptions are worth emphasizing.

First, the model underpredicts mean heights and thicknesses of the Erlangen Bunsen flames characterized by a very low Reynolds number and a low u'/S_L. This result is not surprising, because both the TFC and FSC models were developed based on the Kolmogorov theory of turbulence, which is valid at sufficiently high Reynolds numbers.

Second, both the TFC and FSC models (i) underpredict the influence of the equivalence ratio on the PSI flames and (ii) yield too narrow radial profiles of the mean combustion progress variable when compared to the PSI experiments. These differences are attributed to eventual local combustion quenching and the influence of heat release on turbulence, thus, calling for further investigation of these phenomena.

Moreover, simulations of weakly turbulent flames imply that the simplest linear combination of the gradient source term $\rho_u U_t|\nabla\tilde{c}|$ and the laminar-like source term Q_L on the RHS of Eq. 12 oversimplifies the problem and a more sophisticated combination of these two limit source terms should be developed in order to improve capabilities of the FSC model for predicting turbulent flames associated with $u'/S_L = O(1)$.

Acknowledgments The first (EY) and the third (AL) authors were supported by the Swedish Energy Agency and by the Chalmers Combustion Engine Research Center (CERC). The second author (SV) was supported by TimeTooth Technologies Pvt. Ltd.

References

1. Lipatnikov, A.N., Chomiak, J.: Turbulent flame speed and thickness: phenomenology, evaluation, and application in multi-dimensional simulations. Prog. Energy Combust. Sci. **28**, 1–74 (2002)
2. Veynante, D., Vervisch, L.: Turbulent combustion modeling. Prog. Energy Combust. Sci. **28**, 193–266 (2002)
3. Bilger, R.W., Pope, S.B., Bray, K.N.C., Driscoll, J.F.: Paradigms in turbulent combustion research. Proc. Combust. Inst. **30**, 21–42 (2005)
4. Swaminathan, N., Bray, K.N.C. (eds.): Turbulent Premixed Flames. Cambridge University Press, Cambridge (2011)
5. Echekki, T., Mastorakos, E. (eds.): Turbulent Combustion Modeling. Springer, Berlin (2011)
6. Zimont, V.L., Lipatnikov, A.N.: To computations of the heat release rate in turbulent flames. Doklady Phys. Chem. **332**, 592–594 (1993)
7. Zimont, V.L., Lipatnikov, A.N.: A numerical model of premixed turbulent combustion. Chem. Phys. Reports **14**, 993–1025 (1995)
8. Karpov, V.P., Lipatnikov, A.N., Zimont, V.L.: A test of an engineering model of premixed turbulent combustion. Proc. Combust. Inst. **26**, 249–257 (1996)
9. Prudnikov, A.G.: Burning of homogeneous fuel-air mixtures in a turbulent flow. In: Raushenbakh, B.V. (ed.) Physical Principles of the Working Process in Combustion Chambers of Jet Engines, pp. 244–336. Clearing House for Federal Scientific & Technical Information, Springfield (1967)
10. Zimont, V.L.: Theory of turbulent combustion of a homogeneous fuel mixture at high Reynolds number. Combust. Explos. Shock Waves **15**, 305–311 (1979)
11. Lipatnikov, A.N.: Fundamentals of Premixed Turbulent Combustion. CRC Press, Boca Raton (2012)
12. Lipatnikov, A.N., Chomiak, J.: A simple model of unsteady turbulent flame propagation. SAE Paper 972993 (1997)
13. Lipatnikov, A.N., Chomiak, J.: Transient and geometrical effects in expanding turbulent flames. Combust. Sci. Technol. **154**, 75–117 (2000)
14. Wallesten, J., Lipatnikov, A.N., Chomiak, J.: Modeling of stratified combustion in a DI SI engine using detailed chemistry pre-processing. Proc. Combust. Inst. **29**, 703–709 (2002)
15. Sathiah, P., Lipatnikov, A.N.: Effects of flame development on stationary premixed turbulent combustion. Proc. Combust. Inst. **31**, 3115–3122 (2007)
16. Moreau, P., Boutier, A.: Laser velocimeter measurements in a turbulent flame. Proc. Combust. Inst. **16**, 1747–1756 (1976)
17. Moreau, P.: Turbulent flame development in a high velocity premixed flow. AIAA Paper 77/49 (1977)
18. Magre, P., Moreau, P., Collin, G., Borghi, R., Péalat, M.: Further studies by CARS of premixed turbulent combustion in a high velocity flow. Combust. Flame **71**, 147–168 (1988)
19. Dinkelacker, F., Hölzler, S.: Investigation of a turbulent flame speed closure approach for premixed flame calculations. Combust. Sci. Technol. **158**, 321–340 (2000)
20. Siewert, P.: Flame front characteristics of turbulent lean premixed methane/air flames at high-pressure. PhD Thesis, ETHZ Zürich (2006)
21. Griebel, P., Siewert, P., Jansohn, P.: Flame characteristics of turbulent lean premixed methane/air flames at high-pressure: turbulent flame speed and flame brush thickness. Proc. Combust. Inst. **31**, 3083–3090 (2007)
22. Pfadler, S., Leipertz, A., Dinkelacker, F.: Systematic experiments on turbulent premixed Bunsen flames including turbulent flux measurements. Combust. Flame **152**, 616–631 (2008)
23. Cohé, C., Chauveau, C., Gökalp, I., Kurtuluş, D.F.: CO_2 addition and pressure effects on laminar and turbulent lean premixed CH_4 air flames. Proc. Combust. Inst. **32**, 1803–1810 (2009)
24. Zimont, V.L.: Gas premixed combustion at high turbulence. Turbulent flame closure combustion model. Exp. Thermal Fluid Sci. **21**, 179–186 (2000)
25. Zimont, V.L.: Kolmogorov's legacy and turbulent premixed combustion modelling. In: Carey, W.J. (ed.) New Developments in Combustion Research, pp. 1–93. Nova Science Publishers, New York (2006)
26. Bray, K.N.C., Moss, J.B.: A unified statistical model for the premixed turbulent flame. Acta Astronaut. **4**, 291–319 (1977)
27. Lipatnikov, A.N., Chomiak, J.: A theoretical study of premixed turbulent flame development. Proc. Combust. Inst. **30**, 843–850 (2005)
28. Lipatnikov, A.N., Chomiak, J.: Self-similarly developing, premixed, turbulent flames: a theoretical study. Phys. Fluids **17**, 065105 (2005)
29. Kuznetsov, V.R.: Certain peculiarities of movement of a flame front in a turbulent flow of homogeneous fuel mixtures. Combust. Explos. Shock Waves **11**, 487–493 (1975)

30. Clavin, P., Williams, F.A.: Theory of premixed-flame propagation in large-scale turbulence. J. Fluid Mech. **90**, 589–604 (1979)
31. Launder, B.E., Spalding, D.B.: Mathematical Models of Turbulence. Academic Press, London (1972)
32. Libby, P.A., Bray, K.N.C.: Variable density effects in premixed turbulent flames. AIAA J. **15**, 1186–1193 (1977)
33. Bray, K.N.C.: Methods of including realistic chemical reaction mechanisms in turbulent combustion models. In: Warnatz, J., Jager, W. (eds.) Complex Chemical Reaction Systems. Mathematical Modelling and Simulation, pp. 356–375. Springer, Heidelberg (1987)
34. Lipatnikov, A.N., Chomiak, J.: Molecular transport effects on turbulent flame propagation and structure. Prog. Energy Combust. Sci. **31**, 1–73 (2005)
35. Taylor, G.I.: Statistical theory of turbulence. IV. Diffusion in a turbulent air stream. Proc. R. Soc. Lond. A **151**, 465–478 (1935)
36. Zimont, V.L.: Generalized TFC turbulent premixed combustion model aimed for the ANSYS packages. Sixth Mediterranean Combustion Symposium, June 7–11, 2009. Proceedings
37. Damköhler, G.: Der einfuss der turbulenz auf die flammengeschwindigkeit in gasgemischen. Zs. Electrochem. **46**, 601–652 (1940)
38. Shchelkin, K.I.: On combustion in a turbulent flow. Zhournal Tekhnicheskoi Fiz. **13**, 520–530 (1943)
39. Chaudhuri, S., Akkerman, V., Law, C.K.: Spectral formulation of turbulent flame speed with consideration of hydrodynamic instability. Phys. Rev. E **84**, 026322 (2011)
40. Zimont, V.L., Pagnini, G.: Lagrangian properties of turbulent diffusion with passive chemical reaction in the framework of the premixed combustion theory. Phys. Fluids **23**, 035101 (2011)
41. Wenzel, H., Peters, N.: Direct numerical simulation and modeling of kinematic restoration, dissipation and gas expansion effects of premixed flames in homogeneous turbulence. Combust. Sci. Technol. **158**, 273–297 (2000)
42. Treurniet, T.C., Nieuwstadt, F.T.M., Boersma, B.J.: Direct numerical simulation of homogeneous turbulence in combination with premixed combustion at low Mach number modelled by the G-equation. J. Fluid Mech. **565**, 25–62 (2006)
43. Yu, R., Lipatnikov, A.N., Bai, X.S.: Three-dimensional direct numerical simulation study of conditioned moments associated with front propagation in turbulent flows. Phys. Fluids **26**, 085104 (2014)
44. Maciocco, L., Zimont, V.L.: Test of the TFC combustion model on high velocity premixed CH_4-air combustion in a channel. 20-th Annual Meeting of the Italian Section of the Combustion Institute "Frantic97", Cagliari (1997)
45. Zimont, V.L., Biagioli, F., Syed, K.: Modelling turbulent premixed combustion in the intermediate steady propagation regime. Prog. Comput. Fluid Dyn. **1**, 14–28 (2001)
46. Ghirelli, F.: Turbulent premixed flame model based on a recent dispersion model. Comput. Fluids **44**, 369–376 (2011)
47. Duwig, C., Fuchs, L., Griebel, P., Siewert, P., Boschek, W.: Study of a confined turbulent jet: influence of combustion and pressure. AIAA J. **45**, 624–639 (2007)
48. Keppeler, R., Tangermann, E., Allaudin, U., Pfitzner, M.: LES of low to high turbulent combustion in an elevated pressure environment. Flow Turbul. Combust. **92**, 767–802 (2014)
49. Moreau, V.: A self-similar premixed turbulent flame model. Appl. Math. Model **33**, 835–851 (2009)
50. Halter, F., Chauveau, C., Gökalp, I.: Characterization of the effects of hydrogen addition in premixed methane/air flames. Int. J. Hydrog. Energy **32**, 2585–2592 (2007)
51. Hernández-Pérez, F., Groth, C.P.T., Gülder, Ö.: Large-eddy simulation of lean hydrogen-methane turbulent premixed flames in the methane-dominated regime. Int. J. Hydrog. Energy **39**, 7147–7157 (2014)
52. Kee, R.J., Crcar, J.F., Smooke, M.D., Miller, J.A.: PREMIX: a FORTRAN program for modeling steady laminar one-dimensional premixed flames. Sandia Report SAND85-8249, Sandia National Laboratories, CA (1985)
53. Kee, R.J., Rupley, F.M., Miller, J.A.: CHEMKIN-II: a FORTRAN chemical kinetics package for the analysis of gas-phase chemical kinetics. Sandia Report SAND89-8009, Sandia National Laboratories, CA (1989)
54. Smith, G.P., Golden, D.M., Frenklach, M., Moriarty, N.W., Eiteneer, B., Goldenberg, M., Bowman, C.T., Hanson, R.K., Song, S., Gardiner, J.W.C., Lissianski, V.V., Qin, Z.: GRI-Mech 3.0. http://www.me.berkeley.edu/gri_mech/ (1999)
55. Konnov, A.A.: Implementation of the NCN pathway of prompt-NO formation in the detailed reaction mechanism. Combust. Flame **156**, 2093–2105 (2009)

56. Daniele, S., Mantzaras, J., Jansohn, P., Denisov, A., Boulouchos, K.: Flame front/turbulence interaction for syngas fuels in the thin reaction zones regime: turbulent and stretched laminar flame speeds at elevated pressures and temperatures. J. Fluid Mech. **724**, 36–68 (2013)
57. Sabelnikov, V.A., Lipatnikov, A.N.: A simple model for evaluating conditioned velocities in premixed turbulent flames. Combust. Sci. Technol. **183**, 588–613 (2011)
58. Sabelnikov, V.A., Lipatnikov, A.N.: Towards an extension of TFC model of premixed turbulent combustion. Flow Turbul. Combust. **90**, 387–400 (2013)
59. ANSYS FLUENT 12, Documentation. http://www.ansys.com (2010)
60. Yakhot, V., Orszag, S.A., Thangam, S., Gatski, T.B., Speziale, C.G.: Development of turbulence models for shear flows by a double expansion technique. Phys. Fluids A **4**, 1510–1520 (1992)
61. Shih, T.-H., Liou, W.W., Shabbir, A., Yang, Z., Zhu, J.: A new—eddy-viscosity model for high Reynolds number turbulent flows—model development and validation. Comput. Fluids **24**, 227–238 (1995)
62. Wilcox, D.C.: Turbulence Modeling for CFD. DCW Industries. La Canada, California (1998)
63. Menter, F.R.: Two-equation eddy-viscosity turbulence models for engineering applications. AIAA J. **32**, 1598–1605 (1994)
64. OpenFOAM: Open Source CFD toolbox. http://www.openfoam.com (2011)
65. Launder, B., Sharma, B.: Application of the energy-dissipation model of turbulence to the calculation of flow near a spinning disc. Lett. Heat Mass Transf. **1**, 131–137 (1974)
66. Lipatnikov, A.N., Chomiak, J.: Effects of premixed flames on turbulence and turbulent scalar transport. Prog. Energy Combust. Sci. **36**, 1–102 (2010)
67. Lipatnikov, A.N.: Can we characterize turbulence in premixed flames? Combust. Flame **156**, 1242–1247 (2009)
68. Lipatnikov, A.N.: Conditioned moments in premixed turbulent reacting flows. Proc. Combust. Inst. **33**, 1489–1496 (2011)
69. Lipatnikov, A.N., Sabelnikov, V.A.: Transition from countergradient to gradient scalar transport in developing premixed turbulent flames. Flow Turbul. Combust. **90**, 401–418 (2013)
70. Pope, S.B.: Turbulent Flows. Cambridge University Press, Cambridge (2000)
71. Yeung, P.K., Pope, S.B.: Lagrangian statistics from direct numerical simulations of isotropic turbulence. J. Fluid Mech. **207**, 531–586 (1989)
72. Sreenivasan, K.R.: An update of the energy dissipation rate in isotropic turbulence. Phys. Fluids **10**, 528–529 (1998)
73. Yeung, P.K.: Lagrangian investigations of turbulence. Annu. Rev. Fluid Mech. **34**, 115–142 (2002)
74. Donzis, D.A., Sreenivasan, K.R., Yeung, P.K.: Scalar dissipation rate and dissipative anomaly in isotropic turbulence. J. Fluid Mech. **532**, 199–216 (2005)
75. Tominaga, Y., Stathopoulos, T.: Turbulent Schmidt numbers for CFD analysis with various types of flow field. Atmos. Environ. **41**, 8091–8099 (2007)
76. Bilger, R.W., Saetran, L.R., Krishnamoorthy, L.V.: Reaction in a scalar mixing layer. J. Fluid Mech. **233**, 211–242 (1991)
77. Prudnikov, A.G.: Flame turbulence. Proc. Combust. Inst. **7**, 575–582 (1959)